EPOXY TOUGHENING WITH ORGANIC AND INORGANIC MODIFIERS FOR POTENTIAL USE AS BLAST MITIGATING RETROFITS

A Major Project Report submitted in partial fulfillment for the award of the degree

Of

MASTER OF TECHNOLOGY

In

POLYMER TECHNOLOGY

Submitted by

A.V.ULLAS

(01/PTY/2K10)

Under the able guidance of

DR. P.K.ROY
SCIENTIST 'E'
CENTRE FOR FIRE, EXPLOSIVE AND ENVIRONMENT SAFETY (CFEES)
DEFENCE RESEARCH AND DEVELOPMENT ORGANIZATION (DRDO)
TIMARPUR, DELHI-110054

&

DR. D.KUMAR
PROFESSOR
DEPARTMENT OF APPLIED CHEMISTRY AND POLYMER TECHNOLOGY
DELHI TECHNOLOGICAL UNIVERSITY
(*Formerly Delhi College of Engineering*)
MAIN BAWANA ROAD
DELHI-110042

CERTIFICATE

This is to certify that the M.Tech major project entitled **"Epoxy Toughening with Organic and Inorganic Modifiers for Potential use as Blast Mitigating Retrofits"** has been submitted by A.V.Ullas, for the award of the degree of "Master of Technology" in Polymer Technology is a record of bonafide work carried out by him. Ullas has worked under our guidance and supervision and has fulfilled the requirements for the submission of the dissertation. The project work has been carried out during the session 2011-2012.

To the best of our knowledge and belief the content therein is his own original work and has not been submitted to any other university or institute for the award of any degree or diploma.

DR. D. KUMAR
Professor
Department of Applied Chemistry and Polymer Technology
Delhi Technological University,
Bawana Road, Delhi - 110042

Dr. P.K.ROY
Scientist 'E'
Centre for Fire, Explosive and Environment Safety (CFEES)
Defence Research and Development Organization (DRDO)
Timarpur, Delhi 110054

DR. G.L.VERMA
Professor, Head of the Department
Department of Applied Chemistry and Polymer Technology
Delhi Technological University
Bawana Road, Delhi-110042

ACKNOWLEDGEMENT

I express my sincere thanks and deep sense of gratitude to my supervisor, Dr. P.K.Roy (Scientist 'E', Centre for Fire, Explosive and Environment Safety (CFEES), DRDO) for his inspiring guidance, constant encouragement and motivation throughout the course of this work. To him I owe more than words can say and Dr.D.Kumar (Professor, D.T.U) for guiding and helping me in all ways throughout my course work.

I take this opportunity to convey my sincere thanks to Dr. Sudershan Kumar, Distinguished Scientist and Director, CFEES, DRDO and the management of CFEES for giving me this opportunity to carry out this project work in their prestigious laboratory. It was a privilege to work under the esteemed guidance of Dr. Chitra Rajagopal (Group Head, 'ESG').

I would like to express my profound gratitude to Dr. G.L. Verma (Head of Department, Dept of Applied Chemistry D.T.U) for helping me in all the related problems during the entire duration of M.Tech.

I want to thank Mrs Surekha Parthsarathy, Mr.Rajesh Chopra, Mr. Naveen Saxena, Mr.Saurabh Chaudhary, Ms Manju, Mr.Ankesh and Mr.Javed for their immense support and guidance that helped me in completing the project.

I thank all the members of Centre for Fire, Explosive and Environment Safety (CFEES) for their kind cooperation.

I thankfully acknowledge my family members and friends whose inspiration and motivation brought me to the completion of this project. This was a great learning experience and I will cherish it throughout my life.

Dated (A.V.Ullas)

CONTENTS

TABLE OF FIGURES

LIST OF SCHEMES

LIST OF TABLES

ABSTRACT

In the wake of terrorist attacks, which usually take the form of small bombings, enormous attention has been directed towards development of materials which can be used for mitigation of blast effects. Explosive bombings usually result in damage to the nearby structural elements which hit the occupants of the buildings, leading to human injuries. To prevent the same, suitable multifunctional materials, which can be added as a retrofit layer on existing buildings, are the need of the hour. Although, thick steel panels are capable of providing the requisite level of protection, but in most cases, structures are not designed to support the additional weight requirements which these panels demand. In this project, we have attempted to improve the mechanical properties, in particular the energy absorption characteristics, of epoxy resins by the use of organic and inorganic fillers. The final intention is to use the developed composition as a retrofit layer on the existing unreinforced masonry (URM) structures. Concrete, a common component in all URM, exhibit high compressive strength, but its tensile strength is significantly low, and hence is usually reinforced with materials that are strong in tension (often steel). Retrofitting these structures with polymeric materials can improve the survivability of the walls in the event of a terrorist attack. These polymers can also serve as an additional layer in helmets which can prevent humans from traumatic brain injury. Epoxy resin was chosen as the base polymer and the effect of two different types of fillers on its mechanical properties have been investigated. Since the mixing of inorganic fillers is generally an issue, which necessitates the use of compatibilisers, we have attempted to develop mesoporous substrates, which can reduce the interfacial tension between the two phases. We hypothesized that these mesoporous silicates, due to their extremely high surface area, can lead to substantial improvement in the toughness even at low loadings, without compromising on the tensile strength. Organic modifier, namely amine terminated PEG was also employed as filler and the results are being reported.

CHAPTER 1

INTRODUCTION

The emergence of polymeric materials has changed the face of science and engineering immensely. With the advent of these advanced polymeric materials, light weight and compact structures can be prepared without compromising on the stringent requirements which are required to be met by many engineering products. Several researches have been and are currently underway for the effective utilization of these polymeric materials in various applications. One such application is the area of blast resistance, where tough polymers with high energy absorption characteristic are desirable. The aim of this project is to develop toughened epoxy composites for their use in applications which can withstand dynamic response concerning either blast/shock/impact loadings. These polymers can be added as a retrofit layer on existing structures. The primary function of this layer is to hold back the fragments formed as a result of an explosion in place, so that the injury to the inhabitants of the building can be avoided. One of the greatest threats from blast loading is the fragmentation pieces from walls, windows, equipment, or vehicles flying at high speeds that they can result in extensive injury or death.

The following subsections bring out the complex nature of blast loads, the mechanism of its generation and the efforts which have been directed towards mitigation of blast effects.

1.1. Blast loads

A blast is an enormous wave of air pressure produced by explosion, a wave that destroys everything in its path. There can be many reasons for the occurrence of a blast ranging from natural such as during volcanic eruptions to astronomical in case of supernovae explosion to

chemical, electrical, magnetic, mechanical and of course nuclear. These types of hazards both manmade and natural have the power to completely uproot the normal life of the people by destroying almost everything that comes in its way such as buildings, constructions, etc. Since it is immaterial to talk about the prevention of these volcanic, astronomical explosions, we will restrict ourselves to such type of explosions that can affect buildings only and which is the subject matter of our discussion in this project. Several types of hazards can affect building systems. These hazards can be caused by a human explosion particularly from conventional explosives or the hazards can be caused by a sudden jolt of a strong earthquake or strong winds. Be it an explosion from an explosive or destruction from an earthquake or winds, they all are dynamic in nature because they can be described by their relative amplitudes and relative time (frequency) attributes [1, 2]. Thus, these fall under the broad category of dynamic hazards. Figure 1.1 shows a schematic representation of the amplitude-frequency relationships of several dynamic hazards.

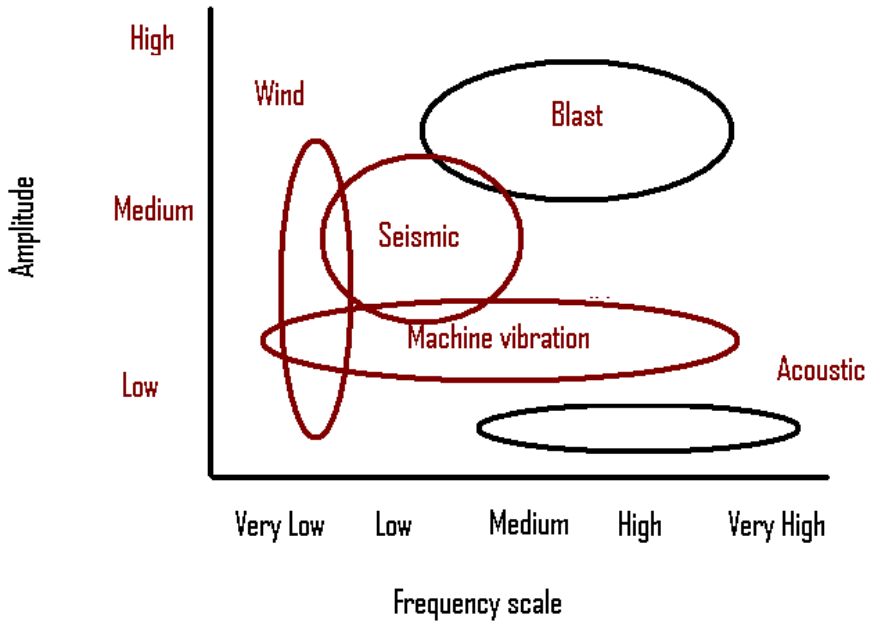

Figure 1.1: Qualitative amplitude-frequency distribution for different hazards

It is very important to highlight the principle differences between static, dynamic and short duration dynamic loads. Static loads do not produce inertia effects in the structural response and are not time dependent, and are assumed to act on the structure for a long period of time (e.g. gravity loads). Dynamic loads, such as induced by earthquakes or wind gusts, have strong time dependencies and their typical durations are measured in tenths of seconds. Short duration dynamic loads are those that are induced by explosions or debris impact and their duration is about a thousand times shorter than the duration of a typical earthquake [3].

An explosion can be understood as a rapid increase in volume and release of energy in an extreme manner, usually with the generation of high temperatures and the release of gases. An explosion occurs when a large amount of energy is suddenly released. This energy may come from an over-pressurized steam boiler, or from the products of a chemical reaction involving explosive materials, or from a nuclear reaction which is uncontrolled. In order for an explosion to occur, there must be a local accumulation of energy at the site of the explosion which is suddenly released. This release of energy can be dissipated as blast waves, propulsion of debris, or by the emission of thermal and ionizing radiation. The speed of the reaction is what distinguishes the explosive reaction from an ordinary combustion reaction. Unless the reaction occurs rapidly, the thermally expanded gases will be dissipated in the medium, and there will be no explosion. The generation of heat in large quantities accompanies most explosive chemical reaction. The exceptions are called entropic explosives and include organic peroxides such as acetone peroxide. It is the rapid liberation of heat that causes the gaseous products of most explosive reactions to expand and generate high pressures. This rapid generation of high pressures of the released gas constitutes the explosion. The liberation of heat with insufficient rapidity will not cause an explosion.

When a chemical compound is formed from its constituents, heat may either be absorbed or released. The quantity of heat absorbed or given off during transformation is called the heat of

formation. Heats of formations for solids and gases found in explosive reactions have been determined for a temperature of 15 °C and atmospheric pressure, and are normally given in units of kilocalories per gram-molecule. A negative value indicates that heat is absorbed during the formation of the compound from its elements; such a reaction is called an endothermic reaction. In explosive technology only materials that are exothermic are of interest. Reaction heat is measured under conditions either of constant pressure or constant volume. It is this heat of reaction that may be properly expressed as the "heat of explosion."

1.2. Mechanism of explosion

A chemical explosive is a compound or mixture which, upon the application of heat or shock, decomposes or rearranges with extreme rapidity, yielding much gas and heat. The reaction must be capable of being initiated by the application of shock, heat, or a catalyst (in the case of some explosive chemical reactions) to a small portion of the mass of the explosive material. A material in which the first three factors exist cannot be accepted as an explosive unless the reaction can be made to occur when needed.

Chemical explosion is the result of the chemical reaction or change of state which occurs over an exceedingly short space of time with the generation of a large amount of heat and generally a large quantity of gas from a small amount of solid. During an explosion, an extremely rapid exothermic transformation takes place resulting in the formation of very hot gases and vapors. Owing to the extreme rapidity of the reaction (one-hundredth of a second), the gases do not expand but remain for a fraction of second inside the container occupying the volume that was once occupied by the explosive charge. As this space is extremely small and the temperature of explosion is extremely high (several thousands of degrees), the resultant pressure is therefore very high (several hundreds of atmospheres), high enough to produce a blast/shock wave which will break the walls of the container and cause damage to the surrounding objects. If the blast wave is strong enough, damage to distant objects can also occur.

The following equation exemplifies how a small nitroglycerine charge of 227 g (Molecular Mass of nitroglycerine) is capable of generating a total of 7.25 moles of total gas, which is equivalent of 162 L at STP (0 °C and 1 atm)

$$4C_3H_5(NO_3)_3(s) \rightarrow 12CO_2(g) + 10H_2O(g) + 6N_2(g) + O_2(g) \quad \Delta H = -5692 \text{ kJ/mol}$$

The pressure generated due to this reaction leads to the formation of a shock wave, which will be discussed in detail the following section.

1.3. Shock wave

A shock wave (also called shock front or simply "shock") is a type of propagating disturbance. Like an ordinary wave, it carries energy and can propagate through a medium (solid, liquid, gas or plasma) or in some cases in the absence of a material medium, through a field such as the electromagnetic field. Shock waves are characterized by an abrupt, nearly discontinuous change in the characteristics of the medium. Across a shock there is always an extremely rapid rise in pressure, temperature and density of the flow. When a high order explosion is initiated, a very rapid exothermic reaction occurs. As the reaction progresses, the solid or liquid explosive material are converted to very hot, dense, high-pressure gas. The explosion products initially expand at very high velocities in an attempt to reach equilibrium with the surrounding air, this cause a shock wave. A shock wave consists of highly compressed air, travelling radially outward from the source at supersonic velocities. A shock wave travels through most media at a higher speed than an ordinary wave. The energy of a shock wave dissipates relatively quickly with distance. Also, the accompanying expansion wave approaches and eventually merges with the shock wave, partially cancelling it out. When a shock wave passes through matter, the total energy is preserved but the energy which can be extracted as work decreases and entropy increases.

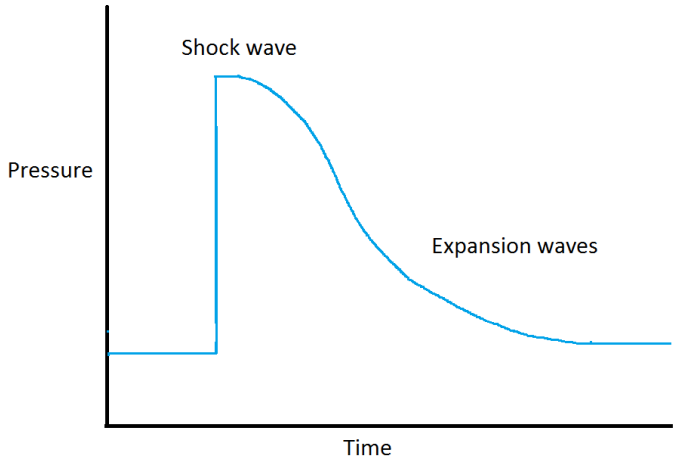

Figure 1.2: Pressure-time diagram at an external observation point for the case of a supersonic object propagating past the observer

It is important here to note the difference between detonation and deflagration. When a loud, sharp bang is heard similar to a grenade or a bomb exploding, it is known as detonation. If the noise is not as loud as that produced by a detonation and is longer in duration and sounds like a hissing sound, it is classified as deflagration. In many cases these effects are preceded and accompanied by fire. If a fire is not accompanied by a thundering noise and 'blowing up' of a building, it is classed as either burning or combustion. Some explosive materials burn relatively slowly (a few millimetres or centimetres per second) if spread on the ground in a thin line. The rate of burning will increase and sometimes develops into deflagration or detonation if these explosive materials are confined. Explosive substances which on initiation decompose via the passage of a shockwave rather than a thermal mechanism are called detonating explosives. The velocity of the shockwave in solid or liquid explosives is between 1500 and 9000 m/s, an order of magnitude higher than that for the deflagration process.

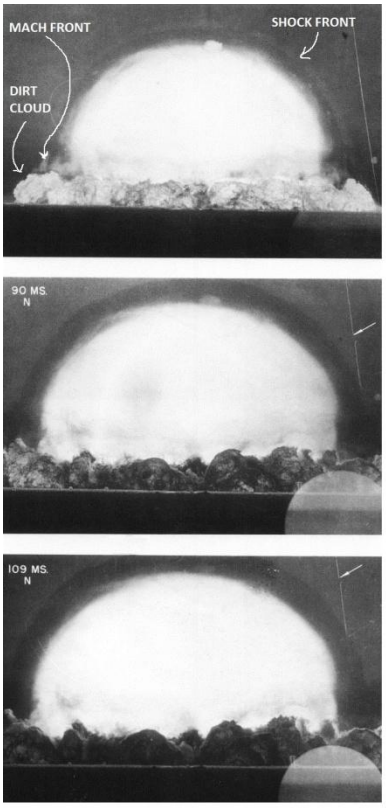

Figure 1.3: Shock wave propagating into a stationary medium, ahead of the fireball of an explosion

Explosive detonations create an incident blast wave which is characterized by an increase in pressure from atmospheric pressure to a peak overpressure (Figure 1.4). As the shock front propagates it takes away with it surrounding air resulting in the formation of a negative pressure that is usually longer in duration than the positive phase. The negative phase is usually less important in a design than the positive phase. As the incident pressure wave strikes a solid object in its path, the wave gets reflected and it transfers the pressure to the object which brings the particle velocity to zero. This is known as reflected pressure. This reflected pressure is always greater than the incident pressure at the same distance from the explosion. The reflected pressure varies with the angle of incidence of the shock wave. When the shock wave strikes a surface that is perpendicular to the direction it is travelling, the point of impact will experience the maximum reflected pressure. When the reflecting surface is parallel to the shock wave, minimum reflected

pressure will be experienced. In addition to the angle of incidence, the magnitude of peak reflected pressure is dependent on the peak incident pressure, which is a function of the net explosive weight and distance from detonation.

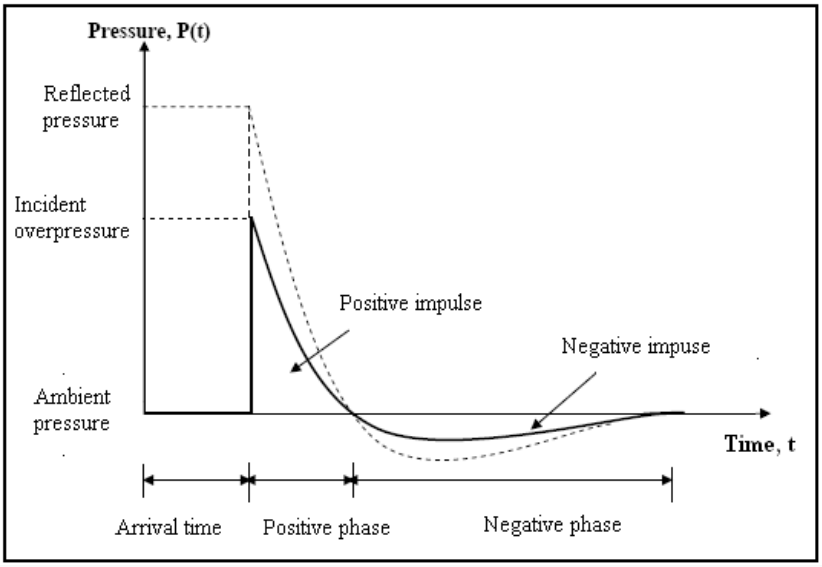

Figure 1.4: Qualitative pressure-time history due to blast loading

When a force of large magnitude acts on a body for a very short interval of time then the product of the force and time is known as the impulse. In other words, impulse is the measure of the energy from an explosion which is imparted to a building. Both the positive and negative phases of the pressure-time waveform contribute to impulse.

1.4. Blast loads on buildings

A blast load on the building will have the following features:

- The intensity of pressure acting on the building can be several orders of magnitude greater than the other hazards. In most cases, the incident peak pressure exceeds 100 psi on a building. At these pressure levels, major damages are expected.

- Explosive pressures decay extremely rapidly with distance from the source. Therefore, the damages on the side of the building facing the explosion may be more severe than on the opposite side.

- The time duration of the event is very short, measured in thousandths of a second or milliseconds. This differs from earthquakes and wind gusts, which are measured in seconds.

The extent and severity of damage and injuries in an explosive event cannot be predicted with perfect certainty. Despite the prevailing uncertainties, it is possible to give some general indications of the overall level of the damage and injuries to be expected in an explosive event, based on the size of the explosion, the stand-off distance and assumptions about the constructions of the buildings:

Table 1.1: The extent of damage with overpressure [4]

Expected extent of damage	Incident Overpressure (psi)
Typical window glass breakage	0.15-0.22
Minor damage to some buildings	0.5-1.1
Panels of sheet metal buckled	1.1-1.8
Failure of concrete block walls	1.8-2.9
Collapse of wood framed buildings	Over 5.0
Serious damage to steel framed buildings	4-7
Severe damage to reinforced concrete structures	6-9
Probable total destruction of most buildings	10-12

Figure 1.5 below exemplify the range-to-effect chart that gives an indication of the minimum distance also known as the stand-off distance necessary to avoid the effects of explosion. It is to be noted that the effects are predominantly a function of the size of the detonating explosive. This type of chart can be used to display the blast response of a building component or window at different levels of protection. A building specific range to effect range-to-effect chart will allow quick determination of the needed stand-off for the amount of explosive in question, after the explosive is decomposed into its products.

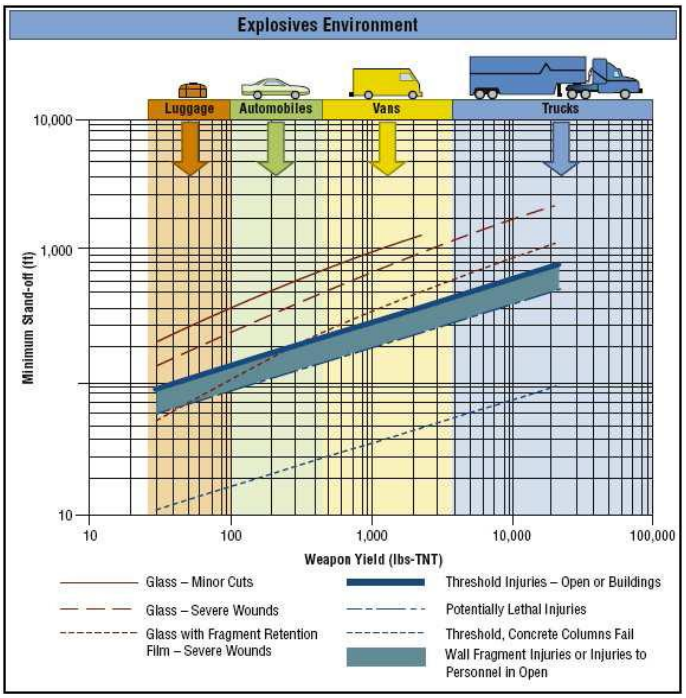

Figure 1.5: Explosives environments-blast range to effects [5]

The air blast shock wave is the primary and the most dangerous weapon of destruction for any building. The shock wave exerts a pressure on the building several orders of magnitude greater than the load bearing capacity of the building (Figure 1.6). The shockwave first engulfs the exteriors of the building which are in close proximity to the shockwaves, progressing inwards into the building air blast waves cause the structures to be pushed both upwards and downwards ultimately ending in floor failure. Floor failure is common in large scale vehicle delivered

explosive attacks and in no time the entire structure becomes vulnerable to the shockwaves and extensive damage occurs within tens to hundreds of milliseconds from the time of detonation.

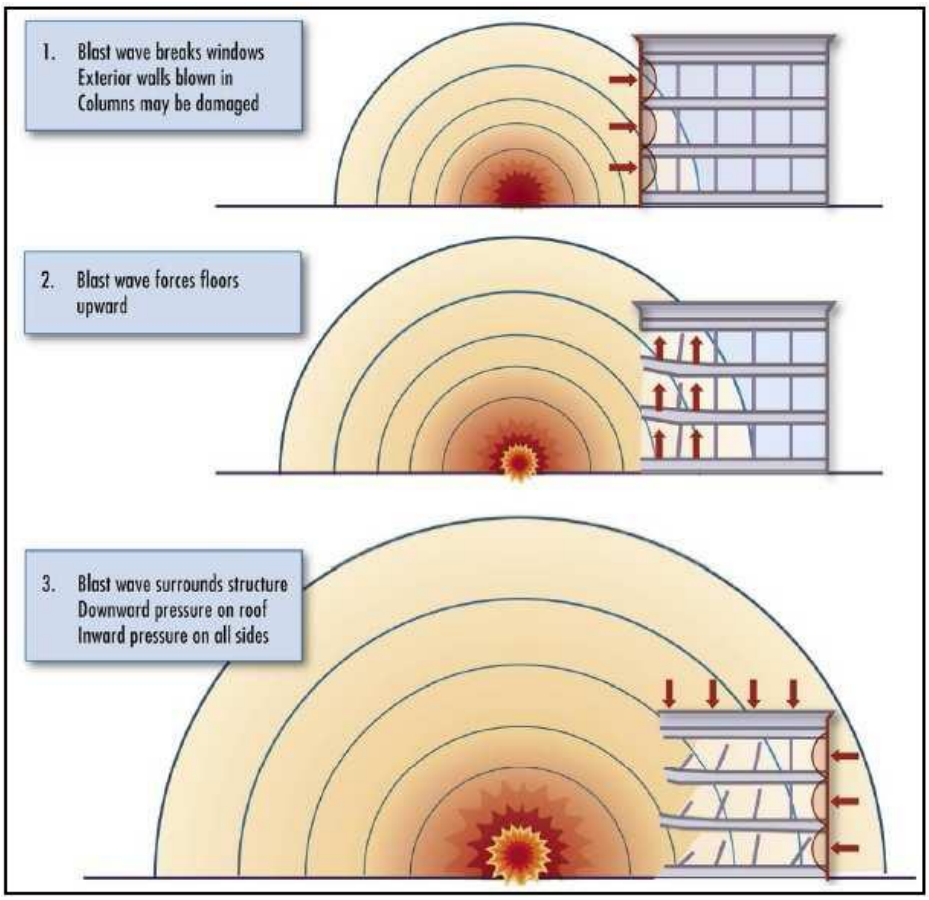

Figure 1.6: Blast pressure effect on a structure

1.5. Improving Blast resistance properties

Un-reinforced masonry (URM) walls have low resistance to out-of-plane loadings, particularly air blast load, due to low flexural capacity and tendency of brittle mode failure. These problems lead to a critical need to develop effective retrofitting techniques to improve the load carrying capacity of such members to resist blast loads. Many studies have been carried out to improve the blast resistance capacity of concrete masonry unit (CMU) walls, including:

1. Adding mass to the walls by increasing thickness with a back up wall comprising of masonry, concrete or some type of steel framing system.

2. Adding vertical steel members as a backup system to greatly reduce the span requirements of the masonry wall system

3. Using fibre reinforced polymer (FRP) composites adhered to the surface of the wall to resist high flexural stresses.

The first two approaches [6, 7] involve significant disruption to the occupants of the building in terms of installation time and loss of usable floor space. Alternatively, experimental investigations on the efficiency of FRP against traditional concrete or steel retrofit have also been performed. Three types of retrofit techniques were used to reinforce the masonry walls: the horizontal FRP rods, the vertical FRP sheets and the horizontal rods with vertical sheets.[6] It was concluded that FRP composites offer greater benefits compared to the first two approaches for strengthening masonry wall's resistance to blast loads.

1.6. Polymers as retrofit materials

In this context, several research groups are working towards improving the ballistic and blast resistance [8] using elastomeric materials. The polymers used for the purpose of retrofitting buildings include polyurea [9, 10], polyurethane and epoxy resins. Polyurea and polyurethanes are prepared by the reaction of isocyanate with polyamines and polyols respectively. Most successful retrofitting compositions are those based on polyurea, the main reason being that the isocyanate-amine reaction is almost instantaneous, which means that retrofitting time can be reduced substantially. However, the spraying of polyurea requires an applicator, where a proportionating unit is used to direct the two components into two separate heated hoses, which lead to a "gun", and the polymerization reaction takes place instantaneously after the material exits the gun. It is to be noted that polyurea is also being advocated as the most suitable material for preventing traumatic brain injury [11-17]. The main reason behind choosing viscoelastic polymeric materials for retrofitting stems from the fact that polymers tend to undergo a transition

from ductile to brittle behavior with increase in the strain rates[18]. During conditions encountered during a blast, the material is subjected to large strain rates, and this transition (from ductile to brittle) takes up a lot of energy leading to improved energy absorption characteristics. In fact, the strain sensitivity of these polymers has been a subject of much research and several visco-elastic models have been introduced in order to explain this behavior. [19, 20]

The base polymer which was chosen for the present project is epoxy as it has been shown to possess higher tensile strength and toughness as compared to polyurea and polyurethanes. The details of epoxy system have been discussed in the following sections.

1.6.1. Thermosetting epoxy resins

Epoxy compounds are one of the most important classes of thermosetting polymers. The resin network has many desirable properties which include high tensile strength, excellent chemical and corrosion resistance and good dimensional stability[21, 22]. As a result, these materials are widely used for applications such as coating structural adhesives, reinforced particles and matrix for advanced composite materials[23-25]. Polyepoxide, known commonly as “epoxy” is a thermosetting polymer formed a result of reaction between an epoxide "resin" with polyamine "hardener". Commercial epoxy resins contain aliphatic, cycloaliphatic or aromatic backbones. They are prepared from either epichlorohydrin or by direct epoxidation of olefins with peracids. The most important intermediate for epoxy resins is the diglycidyl ether of bisphenol A (DGEBA), which is synthesized from bisphenol A and excess epichlorohydrin as per the scheme shown below.

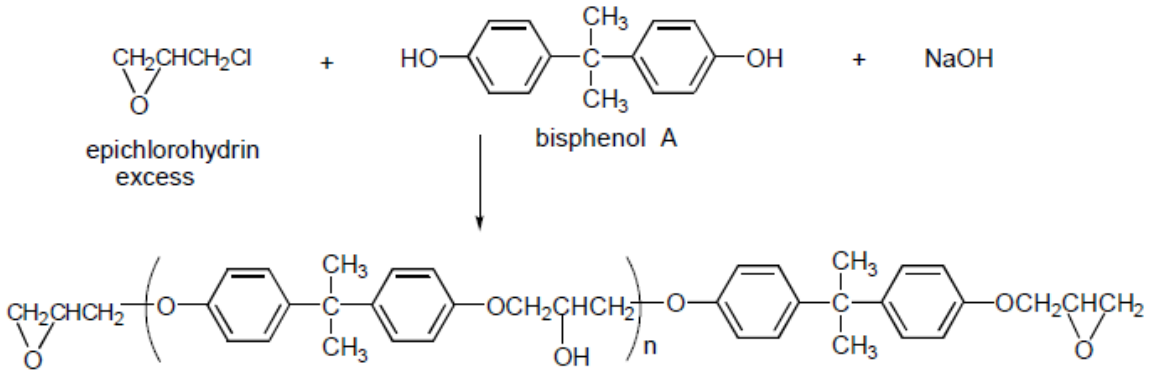

Scheme 1: Synthesis of diglycidyl ether of bisphenol A (DGEBA)

The epoxide ring can react with chemicals with different structures, especially those that have activated hydrogen atoms such as alcohols, amines and carboxylic acids, to mention a few. Treatment of epoxy resins with these agents results in formation of three dimensionally insoluble and infusible networks. The choice of curing agents depends on the required physical and chemical properties, processing methods and curing conditions which are desired. Epoxy resins can be cured with either catalytic or co-reactive curing agents who function as initiators for epoxy ring- opening homopolymerization.

Among chemicals which have the potential to act as curing agents, the primary and secondary amines are the ones which are most commonly employed. Primary amine functionality reacts with an epoxy group to produce a secondary amine and a secondary alcohol. The secondary amine can further react with an epoxy group to form a tertiary amine. Commercial hardeners generally consist of polyamine monomers, a typical example being triethylenetetramine (TETA). Each amine functionality can react with an epoxide group, so that the resulting polymer is heavily cross linked, and results in a formation of a rigid and strong structure. A reaction scheme representing the reaction between the primary amine functionality of TETA with epoxy group is shown in Scheme 2.

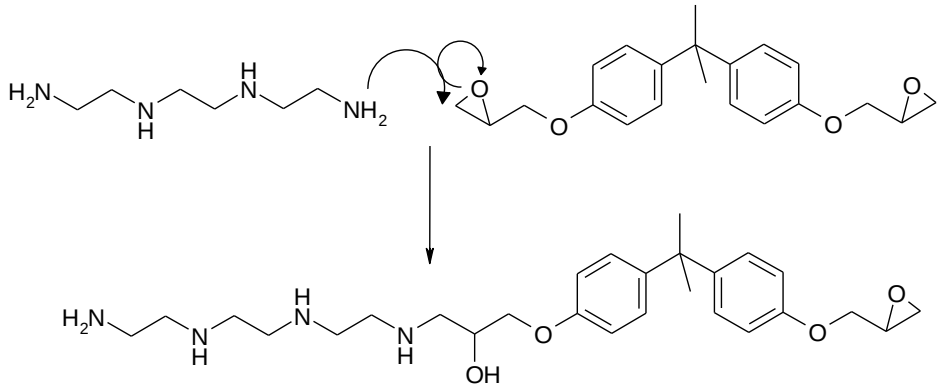

Scheme 2: Reaction scheme of primary amine of TETA with epoxy group

This process is also referred to as "curing", and can be controlled through proper choice of temperature, type of resin and hardener, and the ratio of said compounds. The curing process, which is exothermic, can take minutes to hours for completion. Some formulations benefit from heating during the cure period, whereas others require time and ambient temperatures.

1.7. Improving energy absorption characteristics of polymers

The most important criterion for the selection of material to be used for mitigation of blast effects is its capability of absorbing large amounts of energy. Flexible soft materials that can undergo energy-absorbing molecular rearrangements during deformation are tough, but have less tensile strength. In contrast, rigid hard materials are stiff but also very brittle having little ability to absorb energy, so their toughness is low. To be strong and tough, a material must be able to absorb a large amount of energy during mechanical deformation, without sacrificing its stiffness. Toughness can be defined as the amount of energy per unit volume that a material can absorb before rupturing. In other words, if the polymer undergoes a transition from brittle to a ductile failure on the addition of a secondary phase, then the material is said to have been toughened. Any material which imparts toughness to an epoxy resin is referred to as an “impact modifier”. The area under the stress-strain curve is often used to quantify toughness. Unmodified cured epoxy is inherently brittle and has low shrinkage and high creep resistance, which restrict their

applications in areas which require high impact fracture strength, or even thermal cycle resistance.

1.7.1. Thermoplastic toughening

"Multiple crazing theory" is generally invoked to explain the toughening in thermoplastics. Crazing is defined as the network of fine cracks formed on the surface of a material. A craze is different from a crack in the sense that a craze can continue to support a load unlike a crack. It is assumed that multiple crazes tend to absorb the energy thereby increasing the fracture toughness. Addition of rubber particles both initiate and control the craze growth. This initiation control mechanism is the most widely accepted explanation for toughening in High impact polystyrene (HIPS).

1.7.2. Thermoset toughening

There are three ways of increasing the toughness of thermoset resins.

- *Addition of rubber particles*

In the first instance, the toughening of polymers by addition of rubber particles appears to be the most effective route, but a major drawback is the decrease in the tensile strength of the specimen. The rubbery phase is miscible with the thermoset resin and the curing agents initially, but as cross linking process starts, the rubber particles tend to form a separate layer. Thus, the initially homogeneous solution separates into two distinct phases and this two phase microstructure leads to increased toughness of thermoset resins.

Merz et al. – The rubber particles bridge the opening fracture surfaces at the crack tip and the fracture phenomenon requires the tearing of rubber particles which absorb substantial level of energy thereby exhibiting increased toughness

A tear energy toughening model for the toughening of thermosets has also been proposed[26] . According to this model, the particles stretch across the crack opening behind the crack tip and hinder the advance of crack. According to this model, for a toughened thermoset, the energy absorbed in fracture is the sum of the energy required to fracture a material and to break the rubber particles.[26, 27]

Lately, it has been suggested [28, 29] that the major toughening mechanism is the plastic deformation of the matrix. Plastic deformation blunts the crack tip which reduces the local stress concentration and allows the material to support higher loads before failure occurs. Apart from the above, cavitation of the rubber particles and shear banding of the matrix are also major contributors to the increased energy absorption characteristics of rubber filled thermosets.

When a sample is loaded, the rubber particles experience strong triaxial stresses and thus have a tendency to form a cavity. The cavity is stabilized by good adhesion, often due to chemical covalent bonding between the rubbery domains and the matrix resin; the cavities thus absorb the stresses on the matrix and increase the toughness of the thermosetting polymer. Plastic shear deformation bands are formed as a result of stress concentration in the matrix caused by the presence of rubbery particles. The plastic deformation in modified thermosets is greater than in unmodified thermosets. When a uniaxial stress is applied on the matrix, a triaxial stress acts on the particles, thus plastic deformation occurs and they become localized and leads to the formation of shear bands that initiates at one particle and terminates at the other.

- *Addition of thermoplastics*

Toughening by addition of thermoplastic domains is another way of improving the toughness of thermosets. Many thermosets have been toughened in this fashion [30, 31]. In 1980's, "rigid-rigid polymer alloy concept" was introduced, when substantial toughening was observed in epoxy resins by the addition of a thermoplastic phase. The advantage of using a rigid

thermoplastic phase over a soft rubbery phase is that the modulus remains unchanged and so is the tensile strength. Thermoplastics are used either as granulated particles or as polymers dissolved in the liquid epoxy which later precipitate out as second phase particles. Polyether sulfone (PES)[30], polysulfone[32], polyether imide (PEI), polyphenylene ether (PPE), polybutylene terephthalate (PBT) are some of the thermoplastics that have been used as toughening agents for a variety of thermosetting resins.

- *Addition of fillers*

Introduction of filler particles into the polymer matrix is yet another way of improving the toughness of polymers and in this context both hard and soft fillers have been used to improve the toughness. Epoxy polymers have also been toughened by the addition these fillers[33] and it has also been suggested that the extent of improvement can be varied by altering the shape and size of the fillers introduced. The increase in toughness is explained on the basis of crack pinning mechanism as proposed by Lange et al[34] and later developed by Evan et.al. [35]. According to this model, the toughness improvement was dependent on the volume fraction and particle size of filler. The increase in fracture energy of a brittle material due to the addition of a brittle and second phase was explained by interaction between the propagating crack and the filler phase. When a crack begins to propagate through the resin, the crack front bows between the filler particles but remains pinned at the particles. In this way the growth of the crack is arrested by the addition of fillers. Nanofillers have also been effective in enhancing the impact strength of the fillers reinforced composites [28, 36-38].

1.8. Fillers used for blast mitigation

Several fillers have been evaluated for their potential to improve the blast resistance of polymers including POSS [10], nanoclays, [37, 39], [40], carbon nanotubes [41] [1, 2] to name a few. The use of hollow cylinders has also been proposed as effective fillers for energy absorption [42].

However, because of the incompatible nature of the inorganic filler and organic matrix, most compositions necessitate introduction of a compatibiliser. We hypothesized that this requirement of compatibiliser could be done away with the use of mesoporous materials. We selected representative mesoporous silica (SBA-15) for our investigations. Because of the high surface area which these materials exhibit, a strong interfacial adhesion is expected and the following section deals with the methods used for preparation of such mesoporous silicates.

1.8.1. Mesoporous silica

Mesoporous materials, also known as organic-inorganic hybrid materials are a new class of materials that are characterized by their large surface areas and specific pore sizes. According to IUPAC nomenclature, mesoporous materials are described as those materials whose pore diameter lies in the range of 2-50 nm. Whereas, microporous materials have pore diameter of less than 2 nm and macroporous materials have a pore diameter greater than 50 nm. Mesoporous materials are obtained by the coupling of inorganic and organic components by template synthesis. They are an active area of research particularly with regards to their wide applicability in areas of adsorption, chromatography, catalysis, gas storage, etc. The first of this class of mesoporous materials was synthesized in 1992 under the name M41S. Since then different types of mesoporous materials have been developed such as MCM-41 (Mobil Composition of Matter No. 41), MCM-48, and MCM-50 using different methods. SBA15, (SBA – Santa Barbara University), fifteenth in the class of SBA is a typical mesoporous material having very large surface area and a definite pore size. A silica precursor is used for the preparation of these mesostructured materials along with a structure directing agent, which is usually a surfactant or an amphiphilic copolymer. One necessary condition for the formation of mesoporous silica is an effective interaction between the silica precursor and the structure directing agent so as to form a continuous assembly of hollow tubes having well defined pores.

Ordered mesoporous siliceous materials with controllable mesopore sizes (2–50 nm) are usually assembled from organosilicon alkoxides (e.g. tetraethylorthosilicate, TEOS) [43]. These mesostructured forms of silica show considerable promise as reinforcing agents for several engineering polymer systems at relatively low particle loadings due to the high surface area which can result in favorable interfacial interactions between the polymer and the silica surface[44-46]. Moreover, the pore size of the mesopores is large enough to allow intraparticle diffusion of the polymer inside the filler resulting in a unique composite structure.

For instance, mesoporous silica have been employed as reinforcing agents for epoxy [47, 48], polyimide [49], poly((3-trimethoxysily) propyl methacrylate) [46], poly(vinyl acetate) [50], poly(methyl methacrylate) [51], Nylon 66 [52], polystyrene [53] and polypropylene[54]. Some of these composites exhibited improved tensile strength and tensile modulus as well as marginal improvements in toughness at specific loadings.

1.9. Project aim and objective

This project reveals a novel approach to toughening of the epoxy thermoset by the use of oligomeric structures such as amine functionalized PEG 600 and PEG1500. The effect that these oligomeric structures have on the toughness of epoxy resin is an active area of research and that motivated us to take such a step. It is assumed that PEG will act as a spacer arm and provide flexibility to the polymer thereby absorbing sufficient energy of the blast. The amine functionalized variety of PEG helps to achieve better interfacial adhesion between the matrix and modifier by chemically grafting on to the surface and holding them intact. It is important here to understand that toughness depends to a high extent on the interfacial adhesion between the particle and matrix. Unmodified cured epoxy is brittle, and various thermoplastics, elastomers and fillers have been introduced with an aim to increase the energy absorption characteristics.

More specifically, the objectives of this research are:

- To synthesize and characterize organic and inorganic fillers i.e. amine terminated polyethylene glycols of varying molecular weight and mesoporous silica
- To prepare epoxy composites containing the developed fillers.
- To investigate the effect of increasing loading of the fillers on the mechanical, thermal and structural properties of the composites.
- To determine the effect of increasing strain rate on the mechanical properties of the composites.

CHAPTER 2

EXPERIMENTAL

2.1. Introduction

This section deals with the synthesis and characterization of different types of modifiers for the toughening of epoxy. The details of their preparation as well as their composites with epoxy are also described.

2.2. Materials

HCl (Merck), PEG (CDH), Amino benzoic acid, p- toluene sulphonic acid, pluronic, tetraethylorthosilicate (TEOS) ('AR' grade, E.Merck), isopropanol ('AR' grade, E.Merck), NaOH ('AR' grade, E.Merck). Epoxy resin (Ciba Geigy, Araldite CY 230, epoxy equivalent 200) and hardener (HY 951, amine equivalent 36 eq/kg) was used without further purification. Distilled water was used throughout the course of this work.

2.3. Preparation of mesoporous silica

Mesporous silica was prepared by polymer template technique as per the procedure reported previously[55]. 715 ml of water was mixed with 110 ml concentrated hydrochloric acid and 22 g of PEG-PPG block copolymer (also referred to as P123) was added to it. This was dissolved in the liquid medium by continuous stirring and heating at around 40 ºC for 1 hour. Subsequently, 50 ml of tetra ethyl ortho silicate (TEOS) was added and the resulting solution was stirred for 10 minutes at 40-45 ºC. Stirring was stopped and the mixture was maintained at a constant temperature of 40º C for 24 hours. After the completion of the stipulated period of time, white precipitate was formed; this was washed with distilled water and dried. SBA 15 was obtained by

calcining the precipitate in a furnace at a constant heating rate of 1 ºC min^{-1} upto 600º C. It took 9 hours to complete calcination.

2.4. Synthesis of Amine functionalized polyethylene glycol (AFPEG)

AFPEG was synthesized by reacting poly (ethylene glycol) with 4-amino benzoic acid in the presence of catalytic amounts of p-toluene sulphonic acid (PTSA) as per the procedure reported in the literature [56]. In brief, PEG, 4-amino benzoic acid (2 equivalents /PEG) and excess of xylene were refluxed in a three necked reaction flask fitted with a stirrer and a Dean and Stark trap. The reaction was continued for 15 h, after which no further xylene-water azeotrope could be collected. The reactant mixture was dissolved in chloroform and treated with aqueous saturated sodium bicarbonate solution. Two separate layers were formed and the organic layer containing the amine terminated PEG was collected and dried over anhydrous sodium sulphate. The solvent was subsequently distilled off and the yield was ~ 95%.

2.5. Characterization of fillers

2.5.1. Physisorption studies

The surface area of SBA-15 was determined by nitrogen adsorption-desorption at 77K using a Surface Area Analyzer (Micromeritics ASAP 2010) by. For this purpose the samples were initially outgassed under vacuum (10^{-6} Torr) at 150°C for 16 h and then nitrogen was pulsed at 77K. BET surface areas were calculated from the linear part of the BET plot as per established procedures. [57]

The Barrett–Joyner–Halenda (BJH) method was used to determine the pore size distribution from the desorption branch of the isotherms. Brunauer-Emmett-Teller (BET) method involves the determination of the amount of the adsorbate or adsorptive gas required to cover the external and the accessible internal pore surfaces of a solid with a complete monolayer of adsorbate. This

monolayer capacity can be calculated from the adsorption isotherm by means of the BET equation. The gases used as adsorptives have to be only physically adsorbed by weak bonds at the surface of the solid (van der-Waals forces) and can be desorbed by a decrease of pressure at the same temperature. The most common gas is nitrogen at its boiling temperature (77.3 K). In the case of a very small surface area (below 1 m2/g), the sensitivity of the instruments using nitrogen is insufficient and krypton at 77.3 K should be used.

In order to determine the adsorption isotherm volumetrically, known amounts of adsorptive are admitted stepwise into the sample cell containing the sample previously dried and outgassed by heating under vacuum. The amount of gas adsorbed is the difference of gas admitted and the amount of gas filling the dead volume (free space in the sample cell including connections). The adsorption isotherm is the plot of the amount gas adsorbed (in mmol/g) as a function of the relative pressure p/p_0.

2.5.2. Chemisorption analysis

Ammonia TPD was used to determine the acidity of the silicate filler using chemisorption analyser (Micromeritics Autochem II). For this purpose, mg of sample was saturated with ammonia and it's desorption was studied as a function of temperature.

2.5.3. Structural Characterization

(i) FTIR

The structural characterization of additives was done using FTIR spectroscopy. FTIR spectra were recorded using KBr pellets in the region 400-4000 /cm using a BIORAD (FTS-40) spectrophotometer.

(ii) Scanning Electron Microscopy

SEM analysis of mesoporous silica and the fracture surfaces of epoxy composites were carried out using a HITACHI (S-3700N) scanning electron microscope. The scanning electron microscope (SEM) uses a focused beam of high-energy electrons to generate a variety of signals at the surface of solid specimens. The signals that derive from electron-sample interactions reveal information about the sample including external morphology (texture), chemical composition, and crystalline structure and orientation of materials making up the sample. In most applications, data are collected over a selected area of the surface of the sample, and a 2-dimensional image is generated that displays spatial variations in these properties. Areas ranging from approximately 1 cm to 5 microns in width can be imaged in a scanning mode using conventional SEM techniques (magnification ranging from 20X to approximately 30,000X, spatial resolution of 50 to 100 nm). The SEM is also capable of performing analyses of selected point locations on the sample; this approach is especially useful in qualitatively or semi-quantitatively determining chemical compositions (using EDS), crystalline structure, and crystal orientations (using EBSD).

Principle:

Accelerated electrons in an SEM carry significant amounts of kinetic energy, and this energy is dissipated as a variety of signals produced by electron-sample interactions when the incident electrons are decelerated in the solid sample. These signals include secondary electrons (that produce SEM images), backscattered electrons (BSE), diffracted backscattered electrons (EBSD that are used to determine crystal structures and orientations of minerals), photons (characteristic X-rays that are used for elemental analysis and continuum X-rays), visible light (cathodoluminescence--CL), and heat. Secondary electrons and backscattered electrons are commonly used for imaging samples: secondary electrons are most valuable for showing

morphology and topography on samples and backscattered electrons are most valuable for illustrating contrasts in composition in multiphase samples (i.e. for rapid phase discrimination).

Instrumentation:

Essential components of all SEMs include the following:

- Electron Source ("Gun")
- Electron Lenses
- Sample Stage
- Detectors for all signals of interest
- Display / Data output devices
- Infrastructure Requirements:
    - Power Supply
    - Vacuum System
    - Cooling system
    - Vibration-free floor
    - Room free of ambient magnetic and electric fields

SEMs always have at least one detector (usually a secondary electron detector), and most have additional detectors. The specific capabilities of a particular instrument are critically dependent on which detectors it accommodates.

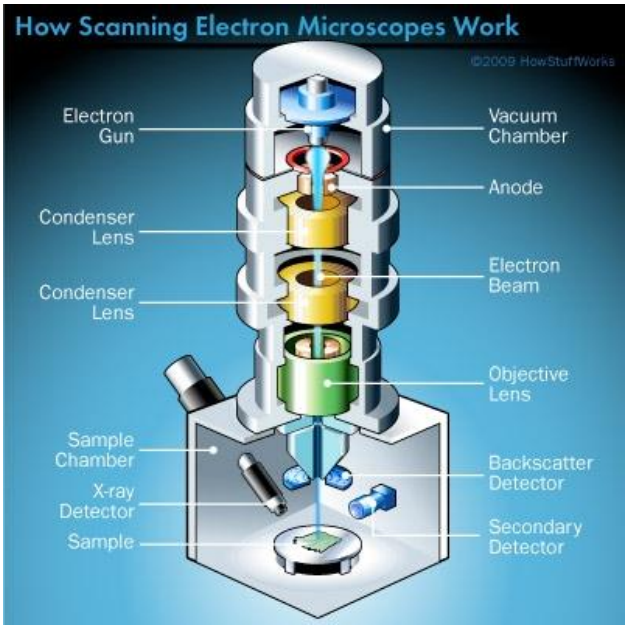

Figure 2.1: Schematic diagram of the working of a scanning electron microscope

(iii) X ray diffraction

XRD of mesoporous silica was done using BRUKER where the diffractograms were recorded over a range of 2θ = 0° to 10°. The wall thickness was calculated as per the procedure reported in the literature: Pore wall thickness = d (100)*2/√3 –pore diameter, where d (100) is the d-spacing value of the (100) diffraction peak in XRD patterns of the silica sample.

X-ray powder diffraction (XRD) is a rapid analytical technique primarily used for phase identification of a crystalline material and can provide information on unit cell dimensions. The analyzed material is finely ground, homogenized, and average bulk composition is determined.

Principle:

Max von Laue, in 1912, discovered that crystalline substances act as three-dimensional diffraction gratings for X-ray wavelengths similar to the spacing of planes in a crystal lattice. X-ray diffraction is now a common technique for the study of crystal structures and atomic spacing.

X-ray diffraction is based on constructive interference of monochromatic X-rays and a crystalline sample. These X-rays are generated by a cathode ray tube, filtered to produce

monochromatic radiation, collimated to concentrate, and directed toward the sample. The interaction of the incident rays with the sample produces constructive interference (and a diffracted ray) when conditions satisfy Bragg's Law ($n\lambda=2d \sin \theta$). This law relates the wavelength of electromagnetic radiation to the diffraction angle and the lattice spacing in a crystalline sample. These diffracted X-rays are then detected, processed and counted. By scanning the sample through a range of 2θangles, all possible diffraction directions of the lattice should be attained due to the random orientation of the powdered material. Conversion of the diffraction peaks to d-spacings allows identification of the mineral because each mineral has a set of unique d-spacings. Typically, this is achieved by comparison of d-spacings with standard reference patterns.

All diffraction methods are based on generation of X-rays in an X-ray tube. These X-rays are directed at the sample, and the diffracted rays are collected. A key component of all diffraction is the angle between the incident and diffracted rays.

Instrumentation:

X-ray diffractometers consist of three basic elements: an X-ray tube, a sample holder, and an X-ray detector. X-rays are generated in a cathode ray tube by heating a filament to produce electrons, accelerating the electrons toward a target by applying a voltage, and bombarding the target material with electrons. When electrons have sufficient energy to dislodge inner shell electrons of the target material, characteristic X-ray spectra are produced. Filtering, by foils or crystal monochromators, is required to produce monochromatic X-rays needed for diffraction. These X-rays are collimated and directed onto the sample. As the sample and detector are rotated, the intensity of the reflected X-rays is recorded. When the geometry of the incident X-rays impinging the sample satisfies the Bragg Equation, constructive interference occurs and a peak in intensity occurs. A detector records and processes this X-ray signal and converts the

signal to a count rate which is then output to a device such as a printer or computer monitor. The geometry of an X-ray diffractometer is such that the sample rotates in the path of the collimated X-ray beam at an angle θ while the X-ray detector is mounted on an arm to collect the diffracted X-rays and rotates at an angle of 2θ. The instrument used to maintain the angle and rotate the sample is termed a goniometer. For typical powder patterns, data is collected at 2θ from ~5° to 70°, angles that are preset in the X-ray scan.

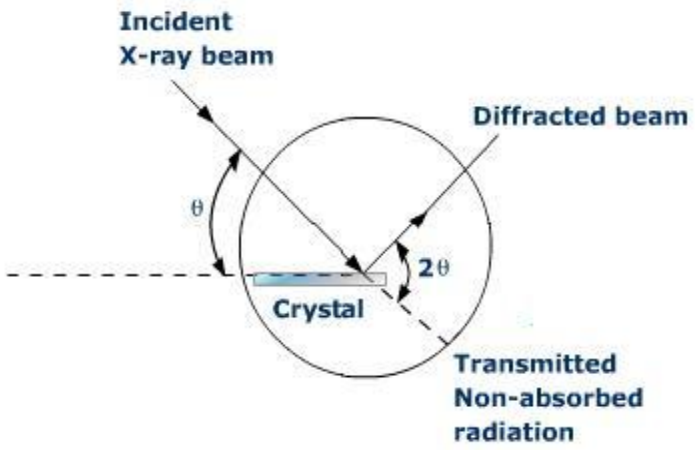

Figure 2.2: Schematic diagram of the working of an XRD

2.5.4. Thermal Characterization

The thermal behaviour of additives was investigated using Perkin Elmer Diamond STG-DTA-DSC in N_2 atmosphere (flow rate=200mL/min) in the temperature range of (50- 600 °C). A heating rate of 10 C/min and sample mass of 3±0.5 mg was used in each experiment.

2.6. Preparation of epoxy composites

Epoxy composites containing amine functionalized PEG, and mesoporous silica was prepared in the presence of TETA hardener. For this purpose, the resin was mixed with requisite amounts of hardener; the amount of hardener used was determined by stochiometry using the formula given by the equation:

$$phr = \frac{AHEW}{EEW} \times 100$$

Where,

AHEW: Amine Hydrogen Equivalent weight, calculated as the ratio of the molecular weight of the hardener to the number of active hydrogen's present. (Appendix 2.1.)

EEW: Epoxy Equivalent Weight (g/eq)

phr: parts per hundred resin

2.6.1. Curing of epoxy resin

The epoxy-hardener mixture, were degassed under vacuum and subsequently transferred to silicone moulds, where the mixture was allowed to cure at room temperature for 24 hours and post cured for 2 h at 150 °C. For preparation of filled samples, epoxy was blended separately with PEG and AFPEG at 5, 10 and 15 phr to form different samples for each modifier. The mixture was degassed to remove entrapped air bubbles and finally poured into silicone moulds for specimen preparation. In case of mesoporous silica, composites were prepared by taking 1, 3, 5 and 7 weight percent of SBA 15 in epoxy matrix. The epoxy matrix containing the additive was ultrasonicated at 33 kHz for 30 min to ensure complete dispersion in the epoxy matrix. Then hardener was added to it, the system was degassed and transferred to moulds for curing and finally testing. Neat epoxy samples were prepared previously to compare the results. The details of all the compositions prepared along with their sample designations are presented in Table 2.1

Table 2.1: Compositional details of the samples prepared

Sample designation	Epoxy (g)	Hardener (g)	Mesoporous silica (g)	AFPEG 600 (phr)	AFPEG 1500 (phr)
EPS	100	13	-	-	-
EPS1	100	13	1.13	-	-
EPS3	100	13	3.39	-	-
EPS5	100	13	5.65	-	-
EPS7	100	13	7.91	-	-
AFG65	100	13	-	5	-
AFG610	100	13	-	10	-
AFG615	100	13	-	15	-
AFG155	100	13	-	-	5
AFG1510	100	13	-	-	10
AFG1515	100	13	-	-	15

2.6.2. Swelling Studies

Swelling tests were conducted for epoxy samples to determine the behaviour of epoxy in various solvents. For this purpose, accurately weighed epoxy samples were placed in different solvents for a period of 72 hours. The samples were weighed periodically to gauge the extent of swelling. To prepare samples for weighing, excess solvent on the sample surface was removed, and then the samples were placed in sealed vials to prevent solvent evaporation during the weighing. At the end of the swelling period, the samples were dried in a vacuum oven at 70 °C for 4 days and weighed again. Percentage change in weight of the samples immersed in different solvents was recorded and reported.

2.6.3. Mechanical Characterization

2.6.3.1. Tensile testing (ASTM D638)

The determination of mechanical properties tensile strength, tensile modulus and strain-at-break were performed at ambient temperature as per ASTM method D638 using an Instron Universal Testing System (3369). Dumb bell shaped specimens were prepared for tensile testing by mixing required amounts of epoxy, hardener and the different modifiers. The dog-bone shaped specimens used in the tensile testing were 90 mm long in the narrow region, 3 mm thick and 10 mm wide along the center of the casting for epoxy resin. The samples were subjected to a cross head speed of 10 mm/min during the tensile tests. At least three specimens were tested to obtain the effective average value of tensile properties.

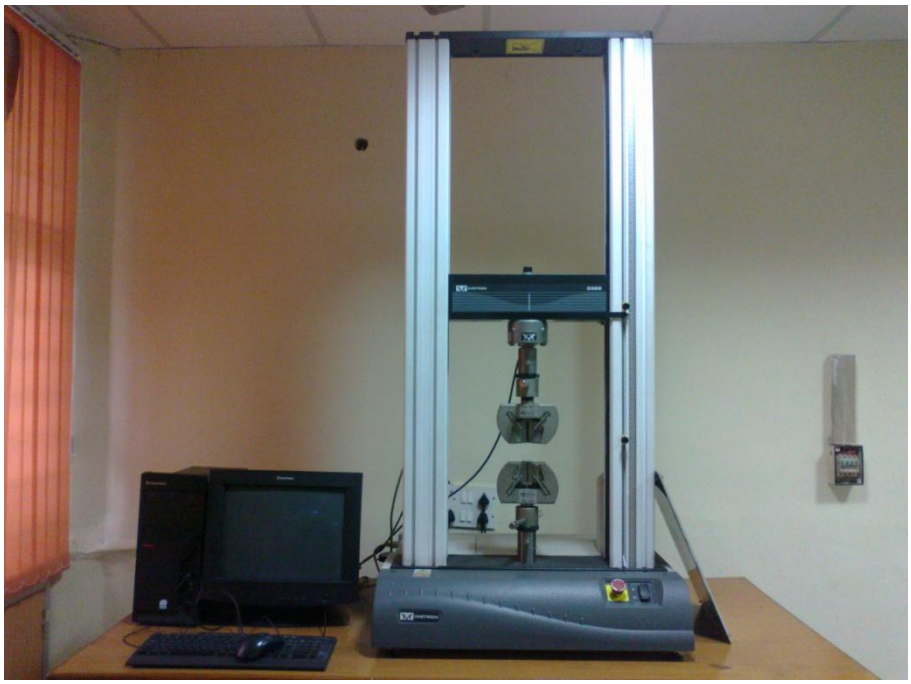

Figure 2.3: Universal Testing Machine (UTM)

2.6.3.2. Impact testing (ASTM D256)

The impact strength of prepared epoxy composites were calculated by Izod system. The energy required to break the samples is a measure of the impact energy of that specimen. Impact strength is found out by calculating the impact energy divided by the thickness of the specimen.

The energy required to break the sample or the impact energy is calculated assuming that the energy lost by the pendulum is equal to the energy absorbed by the test specimen. Impact energy is a measure of the overall toughness of the material. For the purpose of measuring the impact strength of the specimens, the samples were fixed on support vertically and a pendulum bearing weight was allowed to strike the test specimen and break it completely. The samples were placed such that the pendulum was facing the notched side. Notches were made because they act as stress concentrators and facilitate the breaking of samples in one hit of the pendulum. Thus the notched impact strength was noted.

The sample dimension of the specimen for impact testing is given in figure below.

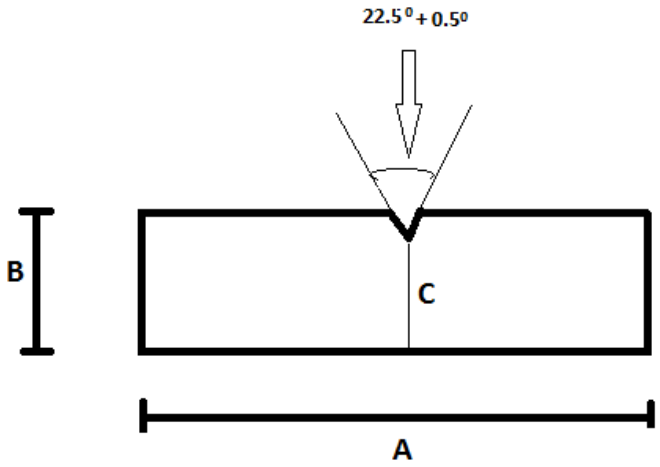

A = 64 mm

B = 12.7 mm

C = 10.2 mm

Notch radius = 0.25 mm

Thickness = 6.4 mm

Figure 2.4: Izod specimen dimensions

2.6.4. High strain rate testing

2.6.4.1. Split Hopkinson Pressure Bar Test

Split Hopkinson Pressure bar is also known as Kolsky bar. It was named after Bertram Hopkinson. This test is used to determine the dynamic stress strain behaviour of materials at high strain rates of 1000 per second – 2500 per second. Since explosion is a type of high impact dynamic loading hence this test is very useful for materials which are potential candidates for retrofitting. The schematic of split hopkinson is presented in figure 2.5. As seen in the figure, it consists of a striker bar, an incident bar and a transmitted bar. Two strain gauges are installed one each on an incident bar and a transmitted bar. The test specimen is sandwiched between the incident bar and the transmitted bar. Split hopkinson test can be performed in tension, compression or torsion mode depending on the requirement. For the purpose of blast simulation, compression test was carried out in the present study.

All the bars are equal in diameter, striker bar is propelled at high speeds using a gas gun to strike the incident bar, and this generates a compression wave, which travels through the incident bar. When the wave encounters a test specimen, it splits up into two small waves one which gets transmitted through the specimen into the transmitted bar and the other which gets reflected back into the incident bar. It is assumed that the specimen undergoes uniform deformation. The incident stress pulse and transmitted stress pulse are measured in real time using two strain gauges installed each on the incident bar and transmitted bar. A stress strain curve is obtained.

The split hopkinson test neat epoxy (EPS) and 1% SBA 15 reinforced epoxy (EPS1) was carried out at TBRL, Chandigarh at strain rates of 1000 per second. The compressive strength of the specimens was recorded.

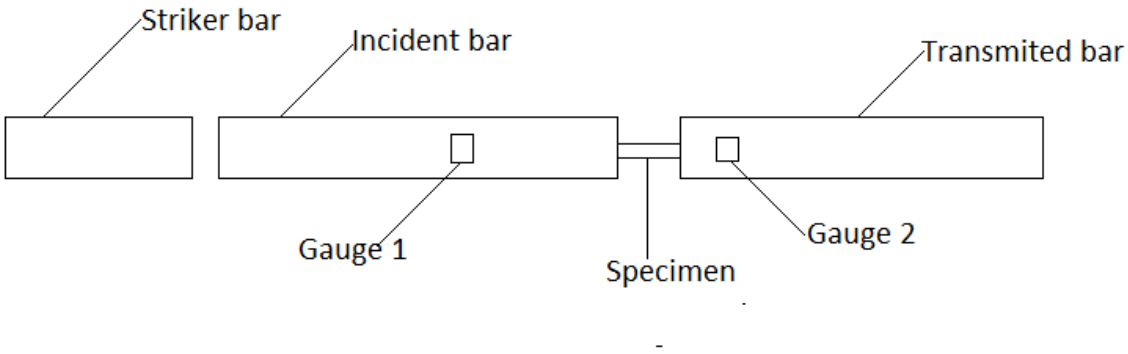

Figure 2.5: Schematic of Split Hopkinson Pressure Bar

CHAPTER 3

RESULTS AND DISCUSSION

This project deals with an approach to improve the energy absorption characteristics of epoxy thermosets. Two different kinds of impact modifiers were prepared; mesoporous silica (SBA-15) and organic modifier i.e. amine terminated polyethylene glycol (ATPEG) and their role towards improvement of the mechanical properties was evaluated.

3.1. Toughening of epoxy with mesoporous silica

3.1.1. Synthesis of mesoporous silica (SBA-15)

Mesoporous SBA 15 exhibiting high surface area and controlled mesoporosity (pore size 5.4 nm) was prepared using a surfactant (amphiphilic polymer) which was later removed by calcination. Structure directing surfactants consist of a hydrophilic part, e.g. ionic, non-ionic, zwitterionic or polymeric groups, often called the “head” and a hydrophobic part, the “tail”, e.g. alkyl or polymeric chains. This amphiphilic character enables surfactants molecules to associate in supramolecular micellar arrays. At very low concentration, the surfactant is present as free molecules dissolved in solvent forming a homogenous solution. They however tend to form aggregates in aqueous solution due to hydrophobic effects. In these aggregates, the surfactant molecules are arranged such that the heads form the outer surface facing the water and the tails are clustered together pointing toward the center. Above a certain critical concentration of amphiphiles, formation of an assembly, such as a spherical micelle, is favored. This concentration is also called the critical micelle concentration abbreviated as CMC. The formation of micelles, the shape of the micelles, and the aggregation of the micelles into liquid crystals depend on the surfactant concentration. At higher concentrations, CMC2, spherical micelles eventually coalesce to form elongated cylindrical rod-like micelles. CMC2 depends strongly on

temperature, surfactant chain length and surfactant counter-anion binding strength. With increasing concentrations, liquid crystalline phases (LC) form. Initially, the rod-like micelles aggregate in hexagonal close-packed arrays. As the concentration increases further, cubic phases form followed by lamellar phases. Details of this sequence might vary, depending on the surfactant, but in general the sequence is valid for most systems. The schematic of the method used is presented in Scheme 3 and Scheme 4.

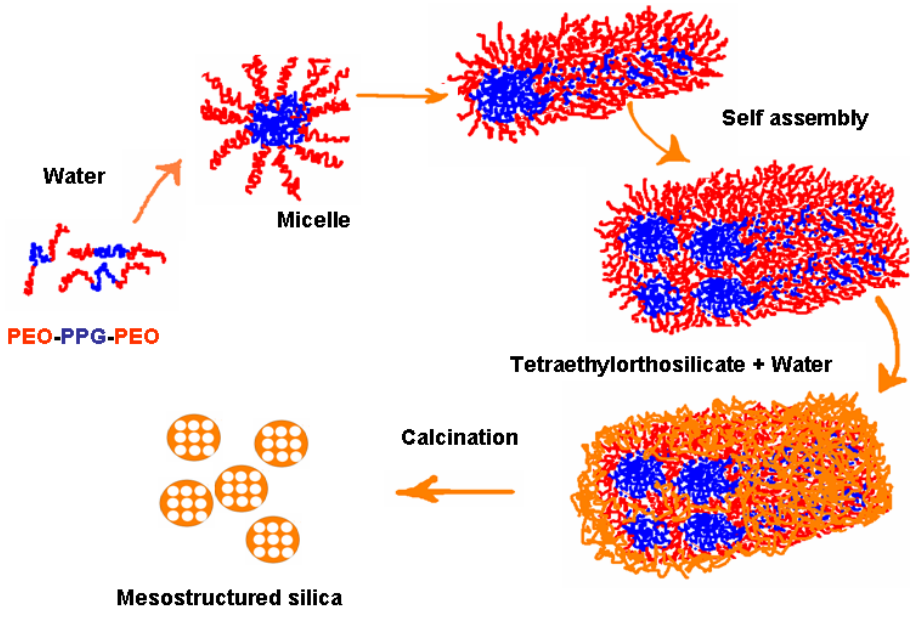

Scheme 3: Schematic for preparation of SBA-15

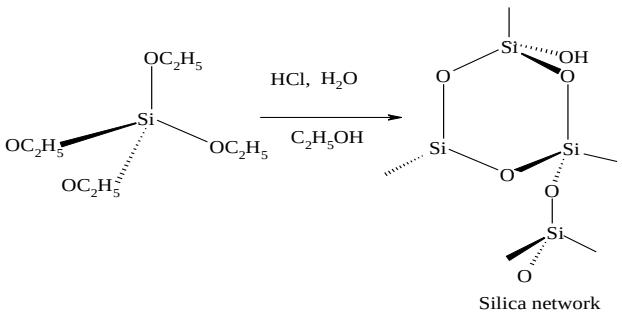

Scheme 4: Reaction scheme for condensation of TEOS

3.1.2. Characterization of mesoporous silica

The texture of the synthesized silicate was determined by SEM imaging which confirm the long hollow rod like structure of the silicate (Figure 3.1). Further structural investigations reveal the presence of pores that are; to be more specific, of mesoporous nature, as is evidenced by the physisorption studies.

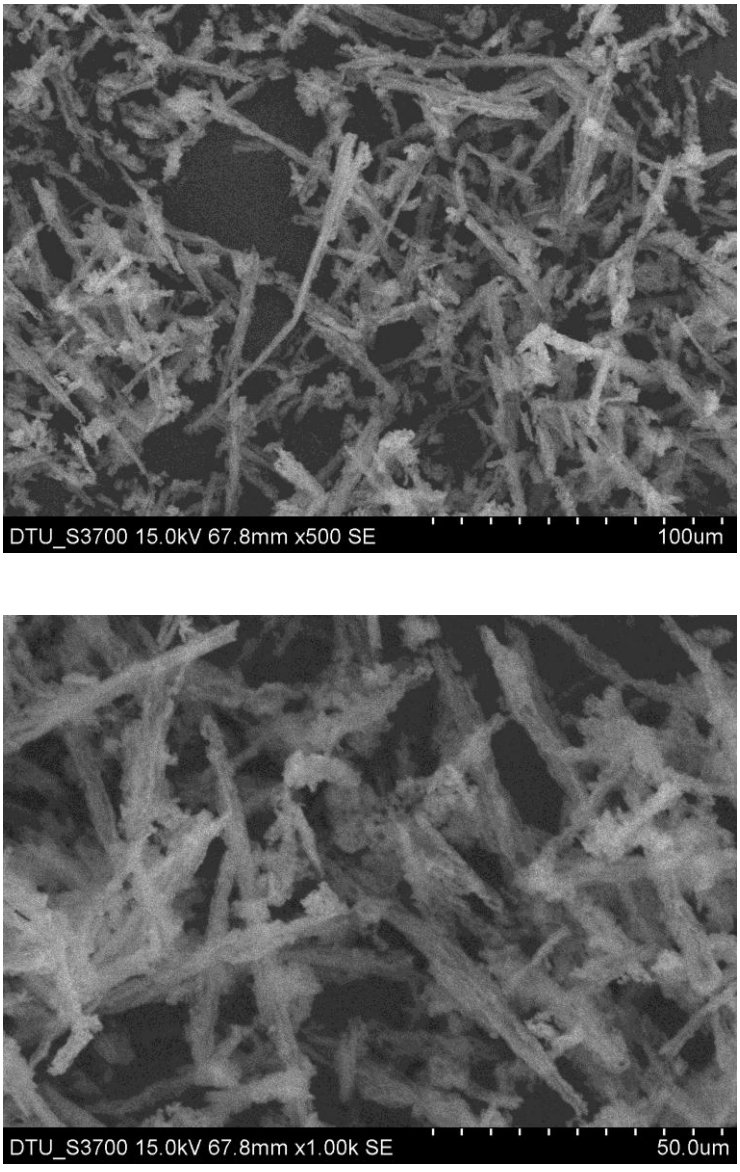

Figure 3.1: Scanning Electron micrographs a) Magnification x500 b) Magnification x1000

3.1.2.1. Surface studies: Nitrogen physisorption

The sample synthesized was subjected to nitrogen adsorption-desorption at 77 K. Nitrogen was adsorbed onto the sample and subsequently desorbed by decreasing the pressure keeping the temperature same. The isotherm is presented in figure 3.2.

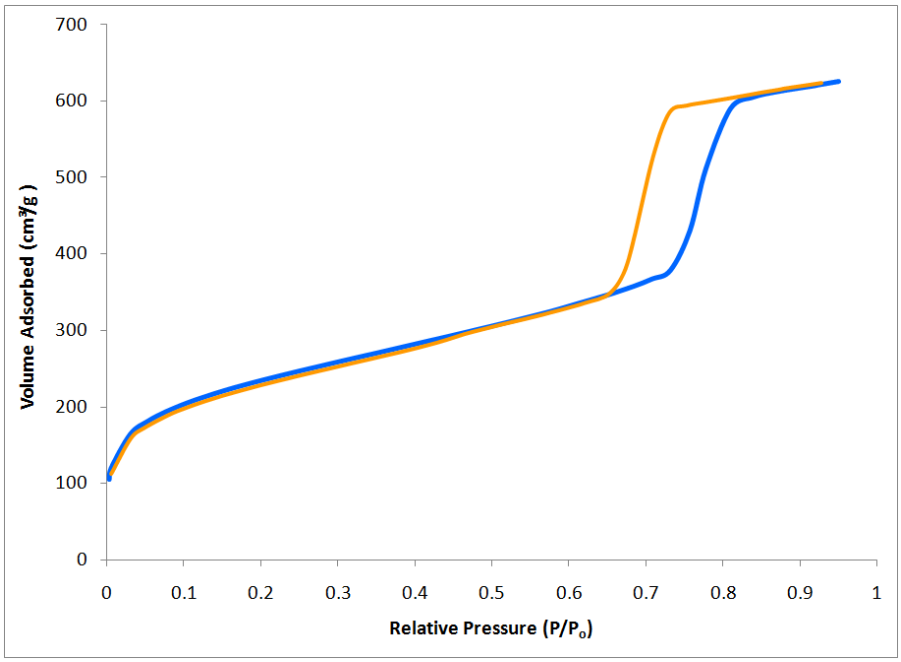

Figure 3.2: N_2 adsorption-desorption isotherms at 77 K

As per IUPAC, there are six types of sorption isotherms which are commonly exhibited by materials and the same are presented in figure 3.3.

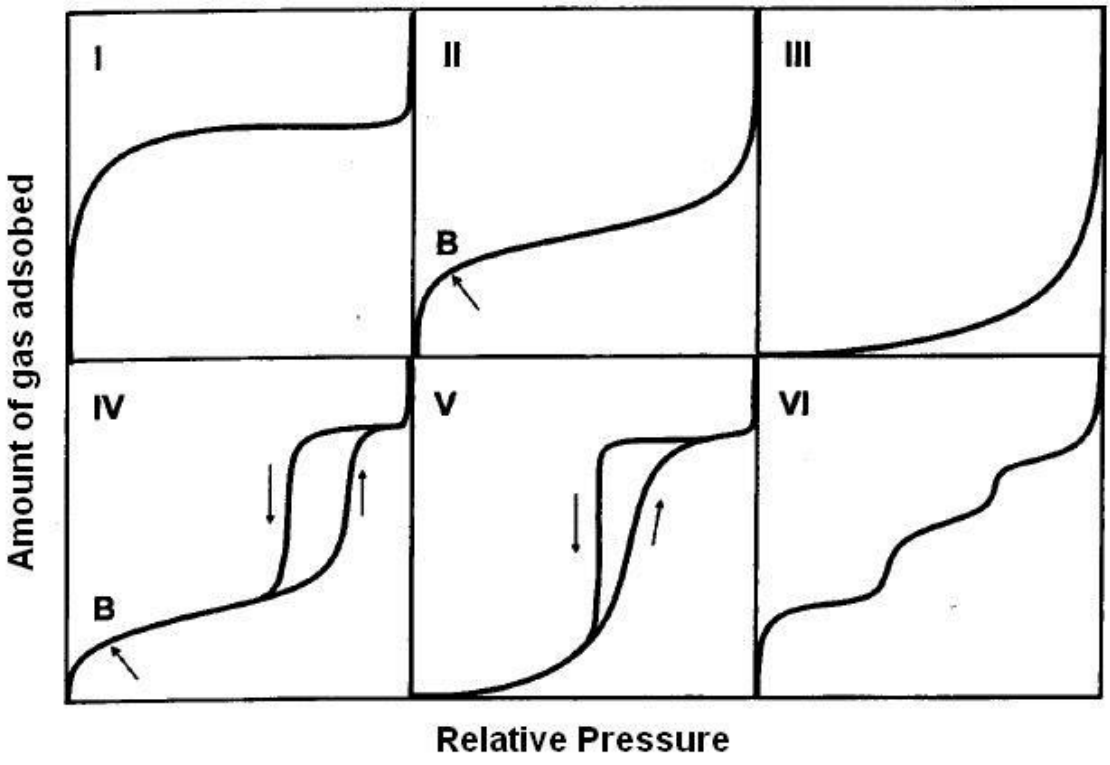

Figure 3.3: Six types of Nitrogen adsorption isotherms [57]

The reversible Type I isotherm is concave to the p/p° axis and n^a approaches a limiting value as p/p°→ 1. Type I isotherms are exhibited by microporous solids having relatively small external surfaces (e.g. activated carbons, molecular sieve zeolites and certain porous oxides), the limiting uptake being governed by the accessible micropore volume rather than by the internal surface area. The reversible Type II isotherm is the normal form of isotherm obtained with a non-porous or macroporous adsorbent. The Type II isotherm represents unrestricted monolayer-multilayer adsorption. Point B, the beginning of the almost linear middle section of the isotherm, is often taken to indicate the stage at which monolayer coverage is complete and multilayer adsorption about to begin. The reversible Type III isotherm is convex to the p/p° axis over its entire range and therefore does not exhibit a Point B. Isotherms of this type is not common; the best known examples are found with water vapour adsorption on pure non-porous carbons. However, there are a number of systems (e.g. nitrogen on polyethylene) which give isotherms with gradual

curvature and an indistinct Point B. In such cases, the adsorbent—adsorbate interaction is weak as compared with the adsorbate—adsorbate interactions. Characteristic features of the Type IV isotherm are its hysteresis loop, which is associated with capillary condensation taking place in mesopores, and the limiting uptake over a range of high p/p°. The initial part of the Type IV isotherm is attributed to monolayer- multilayer adsorption since it follows the same path as the corresponding part of a Type II isotherm obtained with the given adsorptive on the same surface area of the adsorbent in a non—porous form. Type IV isotherms are given by many mesoporous industrial adsorbents. The Type V isotherm is uncommon; it is related to the Type III isotherm in that the adsorbent—adsorbate interaction is weak, but is obtained with certain porous adsorbents. The Type VI isotherm represents stepwise multilayer adsorption on a uniform non-porous surface. The step—height now represents the monolayer capacity for each adsorbed layer and in the simplest case, remains nearly constant for two or three adsorbed layers. Amongst the best examples of Type VI isotherms are those obtained with argon or krypton on graphitized carbon blacks at liquid nitrogen temperature. It can be seen that the calcined silicate (SBA 15) which was prepared by polymer template route possessed mesopores, which was confirmed by a typical type IV hysteresis curve characteristic of these types of materials.

The hysteresis appearing in the multilayer range of physisorption isotherms is usually associated with capillary condensation in mesoporous structures. Such hysteresis loops may exhibit a wide variety of shapes. Two extreme types are shown as HI and H4 in figure 3.4. In the former the two branches are almost vertical and nearly parallel over an appreciable range of gas uptake, whereas in the latter they remain nearly horizontal and parallel over a wide range of p/p°. In certain respects Types H2 and H3 may be regarded as intermediate between these two extremes.

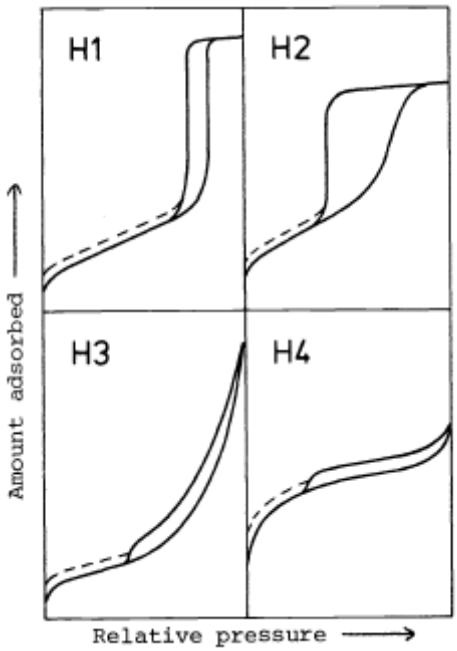

Figure 3.4: Types of hysteresis loops

A feature common to many hysteresis loops is that the steep region of the desorption branch leading to the lower closure point occurs (for a given adsorptive at a given temperature) at a relative pressure which is almost independent of the nature of the porous adsorbent (e.g. for nitrogen at its boiling point at p/p°-0.42 and for benzene at 25°C at p/p° 0.28). The shapes of hysteresis loops have often been identified with specific pore structures. Thus, Type H1 is often associated with porous materials known, from other evidence, to consist of agglomerates or compacts of approximately uniform spheres in fairly regular array, and hence to have narrow distributions of pore size. Some corpuscular systems (e.g. silica gels) tend to give Type H2 loops, but in these cases the distribution of pore size and shape is not well-defined. Indeed, the H2 loop is especially difficult to interpret: in the past it was attributed to a difference in mechanism between condensation and evaporation processes occurring in pores with narrow necks and wide bodies (often referred to as 'ink bottle' pores), but it is now recognized that this provides an over-simplified picture. The Type H3 loop, which does not exhibit any limiting adsorption at high p/p°, is observed with aggregates of plate-like particles giving rise to slit-

shaped pores. Similarly, the Type H4 loop appears to be associated with narrow slit-like pores, but in this case the Type I isotherm character is indicative of microporosity. With many systems, especially those containing micropores, low pressure hysteresis (indicated by the dashed lines in Figure 3.4), may be observed extending to the lowest attainable pressures. Removal of the residual adsorbed material is then possible only if the adsorbent is outgassed at higher temperatures. This phenomenon is thought to be associated with the swelling of a non—rigid porous structure or with the irreversible uptake of molecules in pores (or through pore entrances) of about the same width as that of the adsorbate molecule. Our studies revealed that the SBA-15 synthesized in our lab exhibited a typical, type IV isotherm with H1 type hysteresis loop.

Barrett–Joyner–Halenda (BJH) method was used to determine the pore size distribution from the desorption branch of the isotherms and all the pores were found to have an average diameter of 5.4 nm (Figure 3.5).

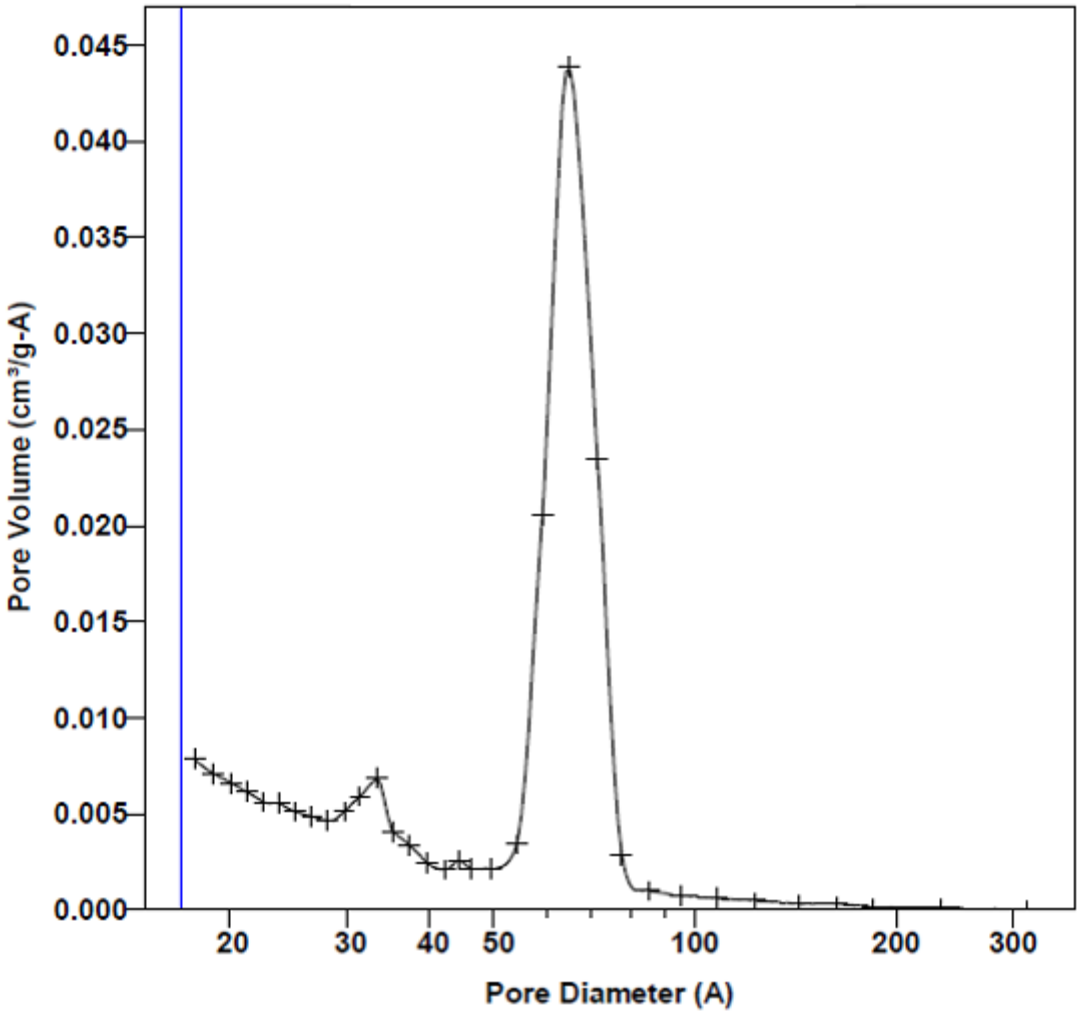

Figure 3.5: BJH framework pore size distribution as determined from the desorption branch

The surface area was determined from the BET equation for which 1/ [VA*(P_0/P-1)] was plotted against relative pressure (p/p_0) (Figure 3.6). Since monolayer formation is reported to be complete at p/p0 =0.3, only those values were used for determination of slope and intercept.

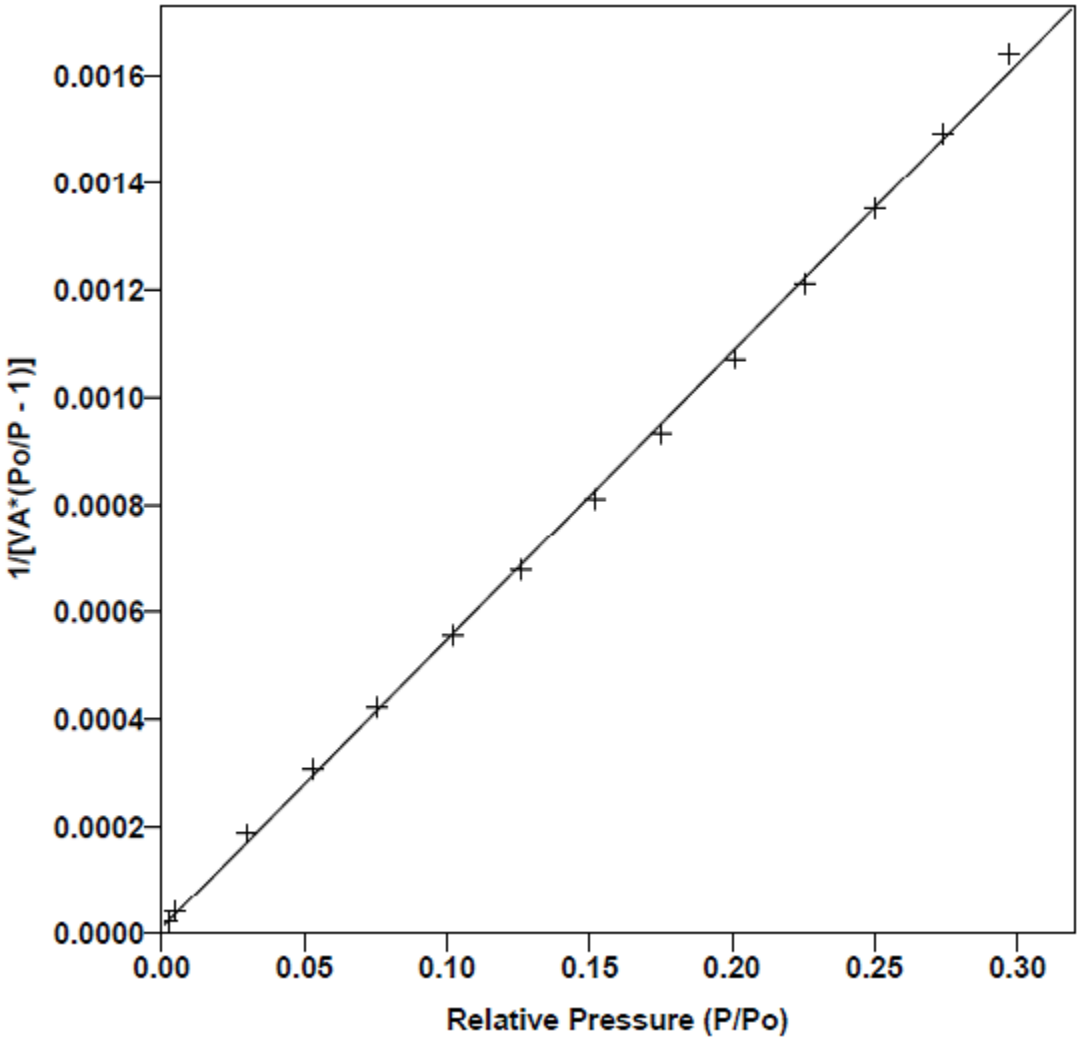

Figure 3.6: BET plot

The equation for determination of surface area is

$$\text{BET Surface Area} = \frac{\text{CSA} \times 6.023 \times 10^{23}}{22414\ \text{cm}^3\text{STP} \times 10^{18}\ \frac{\text{Nm}^2}{\text{m}^2} \times (\text{S} + \text{Y}_{\text{int}})}$$

Where

S = slope of BET plot

Y_{int} = Y intercept

CSA = cross sectional area of nitrogen used as adsorbent

To summarise the physisorption studies, the result are presented in table 3.1.

Table 3.1: Textural properties of mesoporous silica

Sample	**BET surface area /(m^2/g)**	**Langmuir Surface Area/ m^2/g**	**BJH desorption average Pore dia/ nm**	**d(100) / nm**	**Total acidity/ mmol NH_3 g^{-1}**	**Wall thickness/ nm**
SBA -15	808.6	2723.8	5.4	8.8	0.33	4.84

3.1.2.2. Structural characterization: FTIR

The Fourier Transform Infrared spectroscopy (FTIR) of mesoporous silica was carried out on a Fourier transform IR (BRUKER) over the wavenumber range 400-4000 cm^{-1}. The spectrum (Figure 3.5) is similar to the that reported in literature [58], and exhibits characteristic absorption bands at 854 cm^{-1}, which is characteristic of Si-O-Si stretching and another band at 996 cm^{-1} characteristic of Si-OH bending.

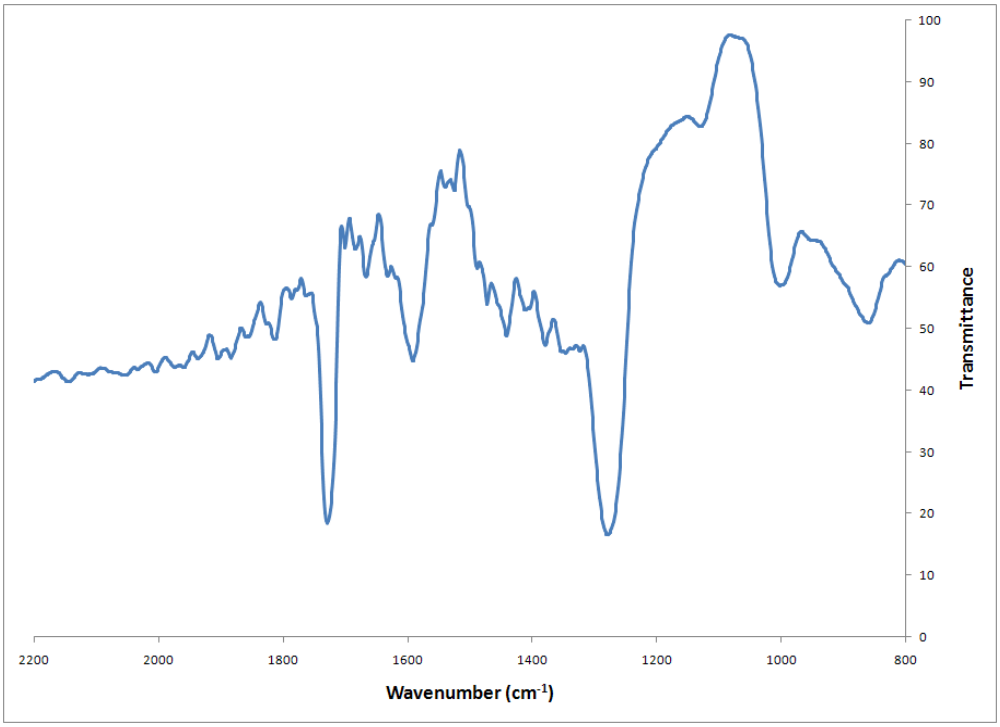

Figure 3.7: FTIR spectra of mesoporous silica

3.1.2.3. XRD

Figure 3.6 shows X-ray diffraction patterns of SBA 15 prepared using the polymer template route. An XRD pattern typical of hexagonal SBA-15 is obtained, with an intense peak at 2θ of 0.3, characteristic of 100 plane. The d (100) spacing was obtained from the diffractogram assuming 1st order diffraction. The obtained value of 8.84 nm matched well with those reported in the literature[58].

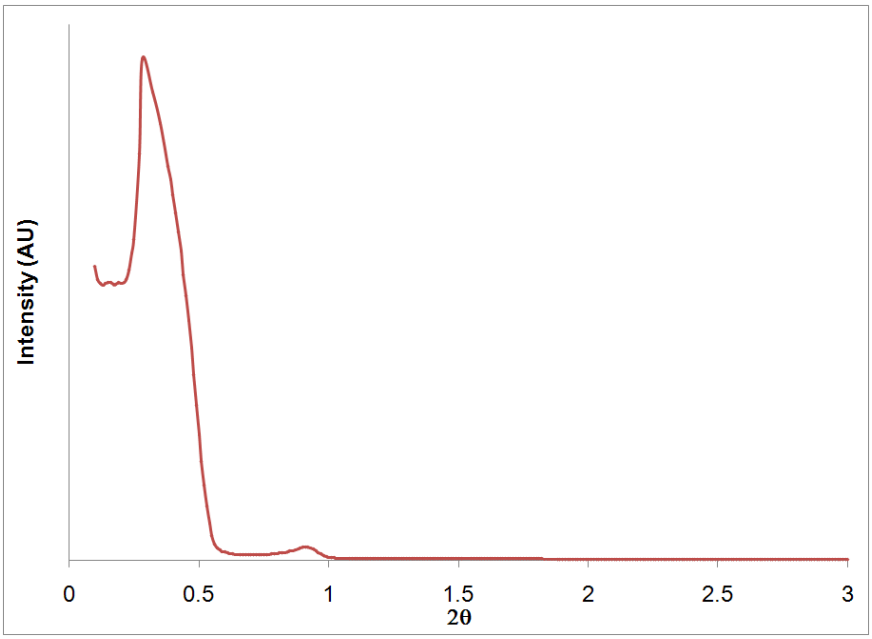

Figure 3.8: X-ray diffraction pattern of SBA-15

3.1.2.4. Temperature programmed desorption

Ammonia TPD was done to determine the total acidity of synthesized siliceous solid. The amount of ammonia desorbed in a characteristic temperature is considered as a measure of the number of acid centers and the temperature range in which the ammonia is desorbed is an indicator of the strength of the acid sites. Experimental TPD-NH_3 profiles of mesoporous silica are shown in Figure 3.9. It can be seen from the figure that desorption of ammonia from the samples starts at 250°C and reaches its maximum at temperatures of ~ 630 °C. The total acidity was measured as 0.33 mmol NH_3 g^{-1}, which is consistent with the results reported in the literature [59]

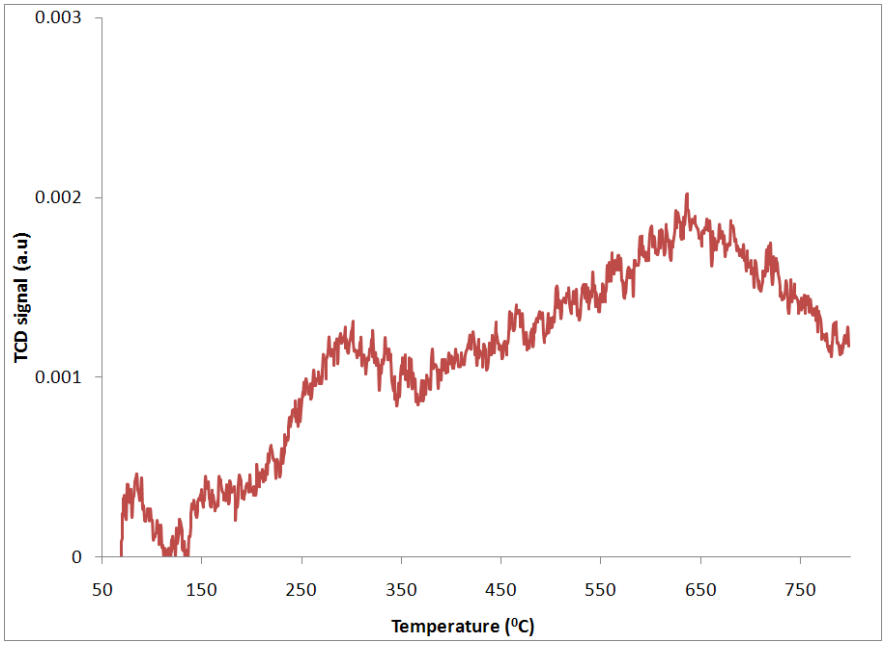

Figure 3.9: Ammonia TPD of SBA-15

3.1.2.5. Thermal characterization

The thermogravimetric trace of the samples before and after calcinations is presented in figure 3.91. The analysis clearly reveals that the calcination process requires a minimum temperature of 600 °C. A programmed heating rate was employed for calcination to ensure that the structure does not collapse in the process. The TGA trace of calcined sample reveals that the surfactant removal is complete. In the TGA trace of calcined silicate, ~2% mass loss during the initial heating period (T<150 °C) is observed. This can be attributed to the removal of water and other condensable species which would have entered the pores of mesostructured silica, because of its extremely high surface area favouring condensation.

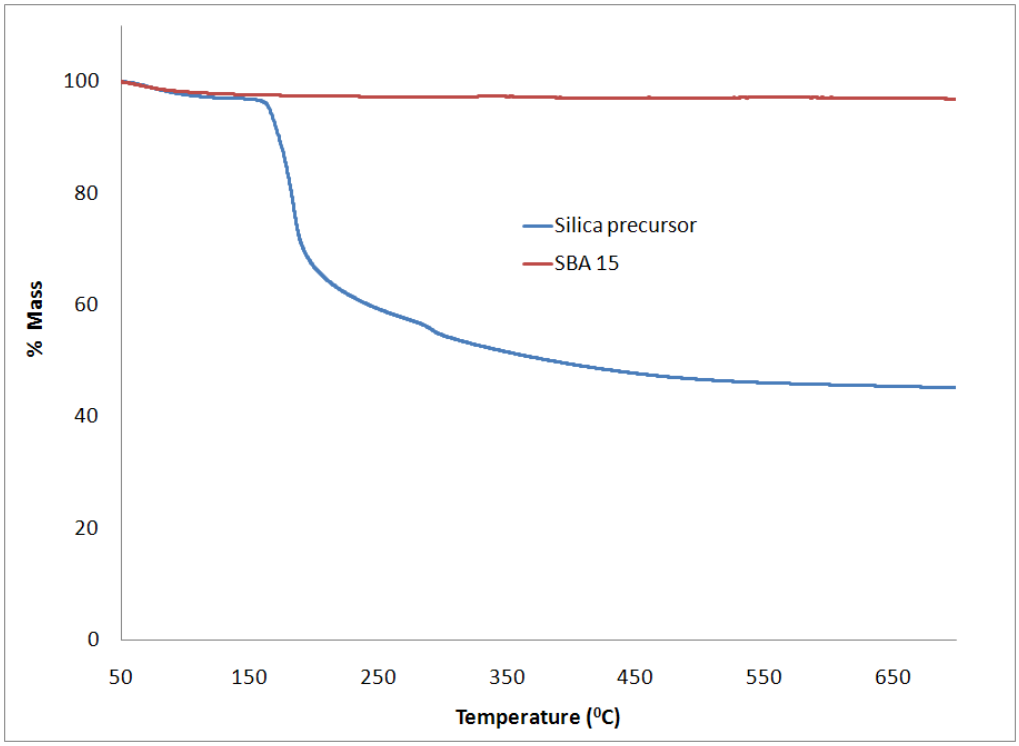

Figure 3.10: TGA traces of silica precursor and calcined sample

3.1.3. SBA 15/Epoxy composites

SBA 15 was dispersed in the epoxy resin by ultrasonication and subsequently hardener was added to cure the resin. The effect of increasing concentration of the filler on mechanical, thermal and structural properties of epoxy resins was studied.

3.1.3.1. Swelling studies

Pre-weighed neat epoxy and its composites were subjected to swelling tests wherein they were immersed in different solvents such as distilled water, methanol, toluene and acetone for a period of 72 hours and reweighed to determine the swelling index. The swelling indexes of different samples are tabulated (Table 3.2). It is to be noted that all the specimens i.e. neat as well as composites were insoluble in the above mentioned solvents. It can be inferred from the table that the extent of swelling was more in case of methanol and toluene as compared to other solvents. All the specimens became brittle on extended exposure to methanol and toluene[60]. As

expected, with increase in the amount of filler, the extent of swelling decreased[61], which may be attributed to the fact that the inert filler did not swell in the medium, thereby not contributing to the swelling index. Interestingly, weight loss was observed when the samples were placed in acetone, which may be due to removal of acetone soluble components present in the sample.

Table 3.2: Results of swelling index of the composites

Solvent	EP	EPS1	EPS3	EPS5	EPS7
Water	1.8	1.4	1.4	1.4	1.3
Methanol	8.2	6.9	5.8	4.8	2.8
Toluene	14.1	8.7	8.6	8.0	8.0

3.1.3.2. Thermal characterization

The TG trace of epoxy and toughened epoxy in the temperature range are presented in Figure. As reported earlier double step decomposition was observed in all the samples[62]. All the samples were stable upto 250 °C. The thermal stability was compared by comparing the initial temperature of decomposition (T_{onset}), final decomposition temperature (T_{end}) and temperature of maximum rate of weight loss (T_{max}) and the results are summarized in table 3.3.

(i) *Initial Decomposition Temperature (T_{onset}):* The temperature at which the first weight loss was observed in the TG trace and was noted by extrapolation.

(ii) *5% decomposition temperature ($T_{5\%}$):* The temperature at which 5 percent decomposition is observed in the TG trace.

(iii) *Final decomposition temperature(T_{end}):* The temperature at which the weight loss virtually stops and is obtained by extrapolation of the final portion of TG trace

(iv) *Temperature of maximum rate of weight loss (T_{max}):* T max was evaluated from the DTG traces. The temperature corresponding to the peak position of derivative plot was noted as T max.

Table 3.3: Results of the thermogravimetric analysis of samples

Sample designation	**$T_{5\%}$ (° C)**	**$T_{onset\ 1}$ (° C)**	**$T_{max\ 1}$ (° C)**	**$T_{onset\ 2}$ (° C)**	**$T_{max\ 2}$ (° C)**	**T end (° C)**
EPS	276.2	344.1	356.1	502.3	539.2	615.2
EPS1	213.2	343	352.1	594.6	545.5	656.8
EPS3	226.5	341.7	354.4	492.6	527.7	655.9
EPS5	227.5	341	352.5	502.8	543.3	656.5
EPS7	227.3	342.8	351.1	487.2	530.1	656.7

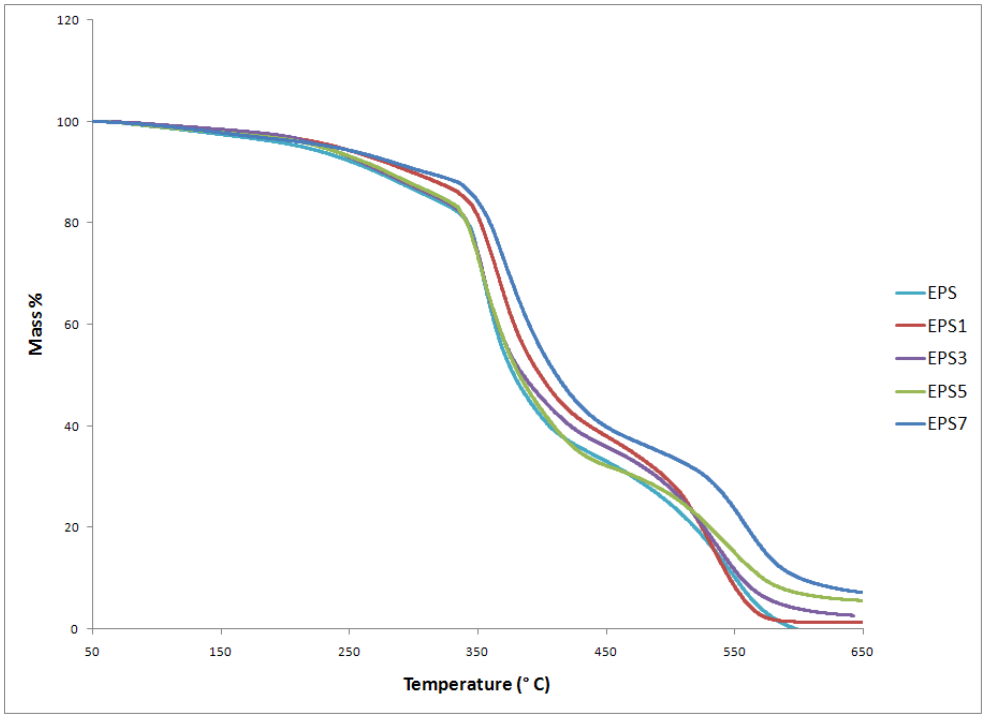

Figure 3.11: TGA traces of neat epoxy and SBA 15 reinforced epoxy

3.1.3.3. Mechanical properties

3.1.3.3.1. Quasi-static testing: Tensile testing (ASTM D638)

Dumb bell shaped specimens were prepared as reported in the experimental section. The photographs of representative samples are shown in Figure 3.12.

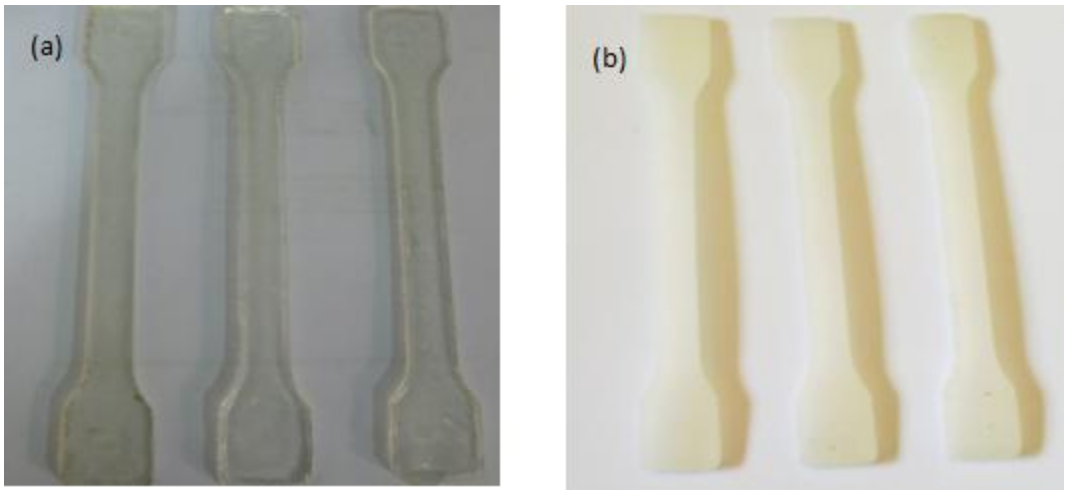

Figure 3.12: Photographs of samples a) neat Epoxy b) SBA 15 reinforced epoxy

The composites were tested for their mechanical behavior at low strain rates (10 mm per minute) on a universal testing machine for determination of their tensile properties. The results have been summarized and are presented in Figure 3.13-3.15. It can be seen that the characteristic tensile properties of the polymer were improved at lower silica loadings (1% w/w) which is probably the result of homogeneous dispersion of the filler within the matrix.

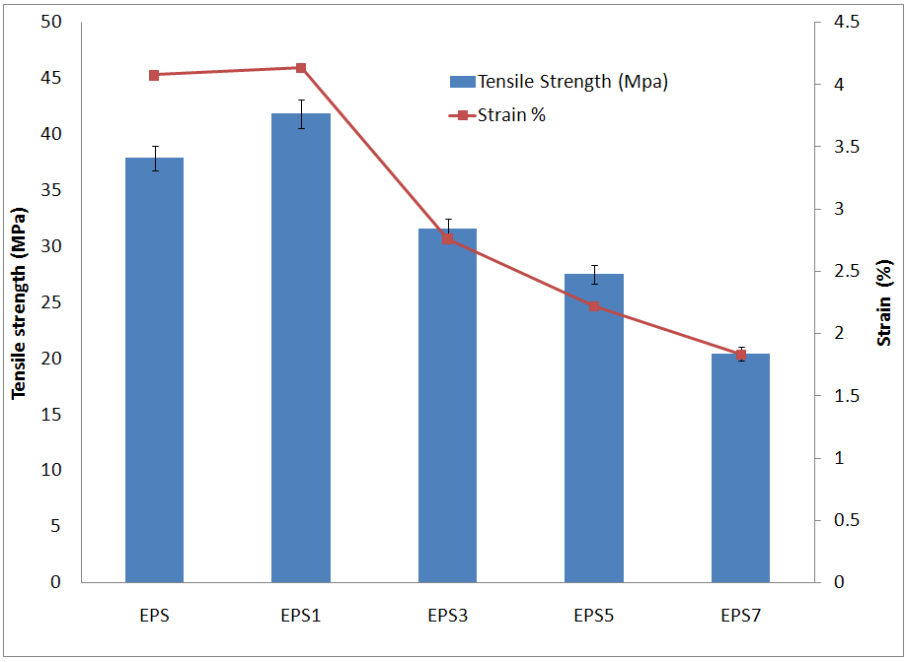

Figure 3.13: Variation in tensile strength and strain with increase in silica loading

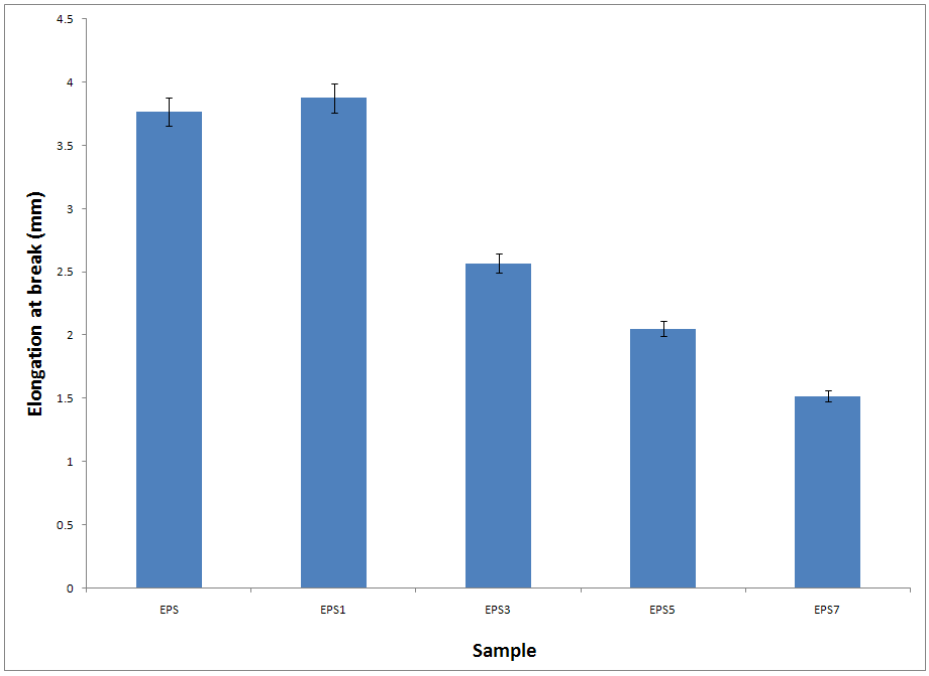

Figure 3.14: Elongation at break of epoxy composites

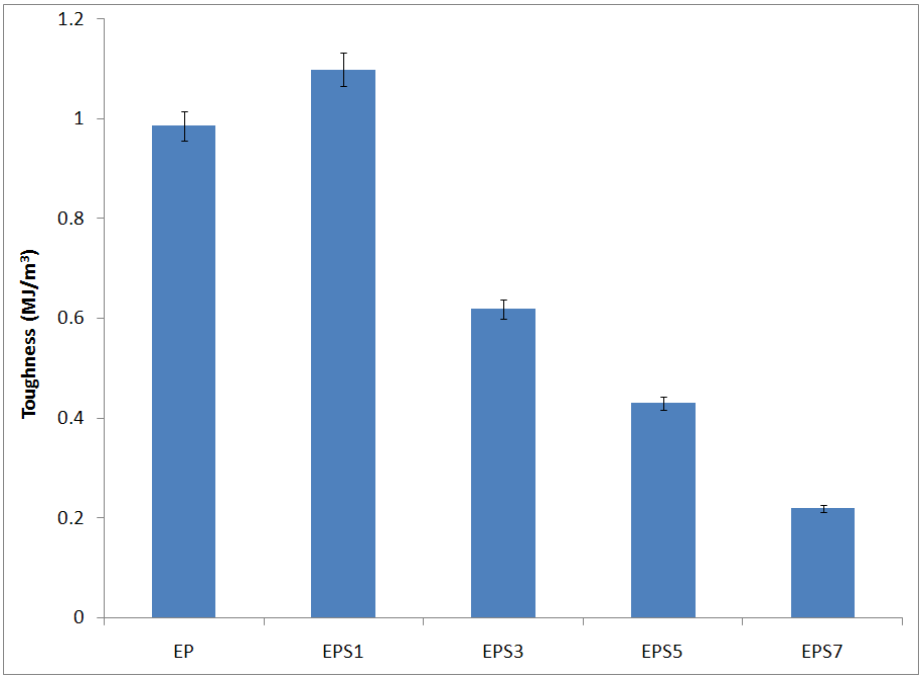

Figure 3.15: Variation of toughness with increase in SBA 15 loading

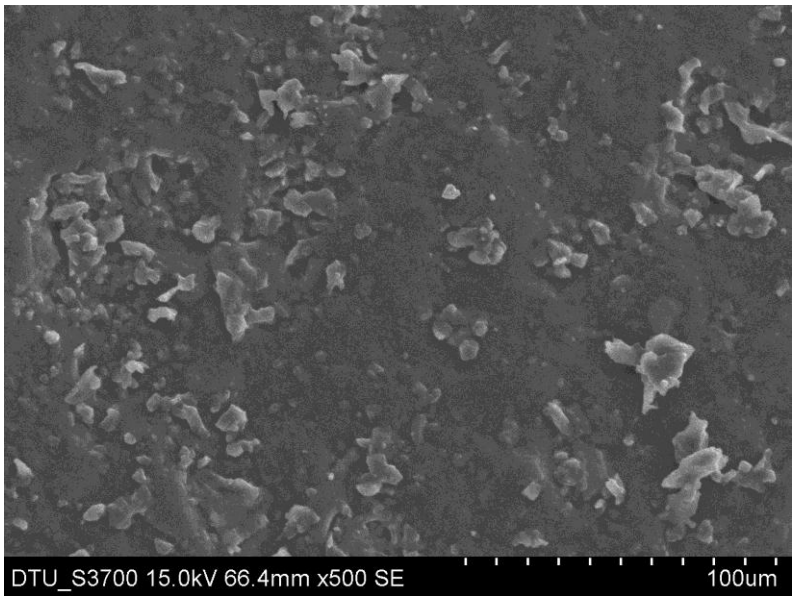

Figure 3.16 (i): SEM of the fractured surface of neat epoxy specimen

Owing to the large surface area and the uniform pore size distribution of the silica mesostructure, which can allow intraparticle diffusion, we anticipated an improvement in the tensile properties of the composite. For the purpose of toughness measurements, the total area under the stress strain curve till complete fracture was determined and has been reported. It is to be noted that the average pore diameter of SBA 15 is sufficiently large (5.4 Å) so as to allow the penetration of both resin and hardener into the pores resulting in the formation of a cured matrix within the pores, thereby leading to its improved properties. [63, 64]

What is interesting to note is the change in the fracture mechanism due to the introduction of the siliceous filler. The SEM images of the fractured surfaces are presented in figure 3.14, which clearly show that the neat epoxy specimens fractured in a brittle manner.

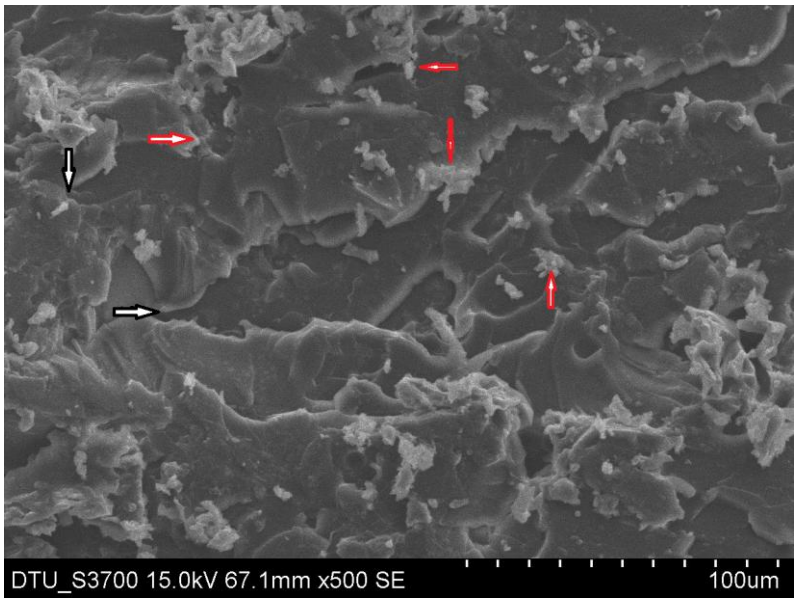

Figure 3.16 (ii): SEM of the fractured surface of SBA 15 reinforced epoxy specimen at 1 %(w/w) loading

The two figures above gives us a clear understanding of what is actually happening during stress loading. The SEM photograph of unmodified epoxy reveal that when the material is loaded above its limit, the crack propagates in a direction perpendicular to the direction of loading and fractures it in a brittle manner but in the case of SBA 15 reinforced epoxy, when a crack front propagates through the matrix, it encounters a silica particle, thus micro cracks are formed. The arrow in white colour shows the development of micro cracks. The growth of micro cracks is arrested by the presence of silica particles as shown by the arrow in red. We believe that the introduction of silica hinders the propagation of the crack, a phenomenon more commonly known as the crack pinning, which lead to the failure of the specimen in a ductile fashion thus leading to increased energy absorption by the composite[34]. According to this model, the increase in fracture energy due to addition of the second phase is explained on the way the propagating crack interacts with the filler. The propagating crack front bows out between the filler particles but remains pinned at the particle, thereby arresting the growth of the crack.

3.1.3.3.2. Low velocity impact testing: Izod (ASTM D256)

Low velocity impact testing was performed on SBA 15- epoxy composites to determine the amount of energy absorbed by the specimen at low impact rates. The results of izod impact testing are given in figure below (Figure 3.17). It was seen that that there was an increase in the impact strength of EPS1 as compared to EPS. However, the impact strength decreased as the weight percent of SBA 15 loading increased. The reduction of impact strength at higher filler content may be due to the agglomeration of the particle. These agglomerates are the weak link and break fairly easily when force is acted on it.

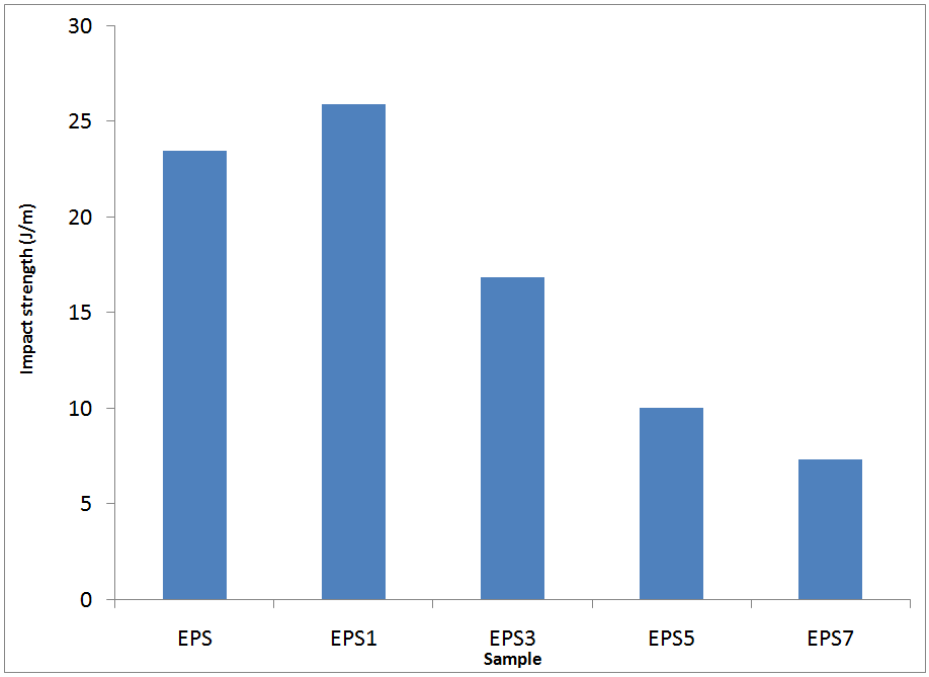

Figure 3.17: Impact strength of composites

3.1.3.3.3. High strain rate testing

The compressive testing of neat epoxy and composite containing SBA 15 (1 % w/w) were characterized at high strain rates. Two samples from each configuration were tested at high strain rates of 1000 per second in a Split Hopkinson bar at TBRL Chandigarh.

The results of the compressive strengths of the materials are reported below in Table 3.4:

Table 3.4: Compressive strengths of the specimens at strain rate of 1000 per second

Sample	Compressive Strength (MPa)
EPS	120
EPS1	120

3.2. Organic: Toughening of epoxy with amine functionalized PEG

3.2.1. Determination of amine content

The amine content of amine functionalized PEG 600 and PEG 1500 was determined by taking weighed amounts of sample in an isopropanol/water ratio of 80 : 20 and titrating the contents against 1.1 N HCl using the presence of a few drops of bromophenol blue as indicator.

The amine content was calculated as

$$\text{Amine content} = \frac{\text{Normality} \times \text{Titre value (ml)}}{\text{Sample weight (g)} \times 1000}$$

The amine content of amine functionalized PEG 1500 was found to be 1.6 eq/kg

The amine content of amine functionalized PEG 600 was found to be 2.1 eq/kg

3.2.2. Structural characterization: FTIR

The FTIR analysis of amine functionalized PEG samples were carried out on a Fourier Transform IR at a wavelength range from 400 – 4000 cm^{-1}. The FTIR spectra of PEG and aminated PEG is presented in Figure 3.18. A –C=O stretching band at 1700cm^{-1} is observed in the case of aminated derivative, which supports the conversion of the PEG into its ester.

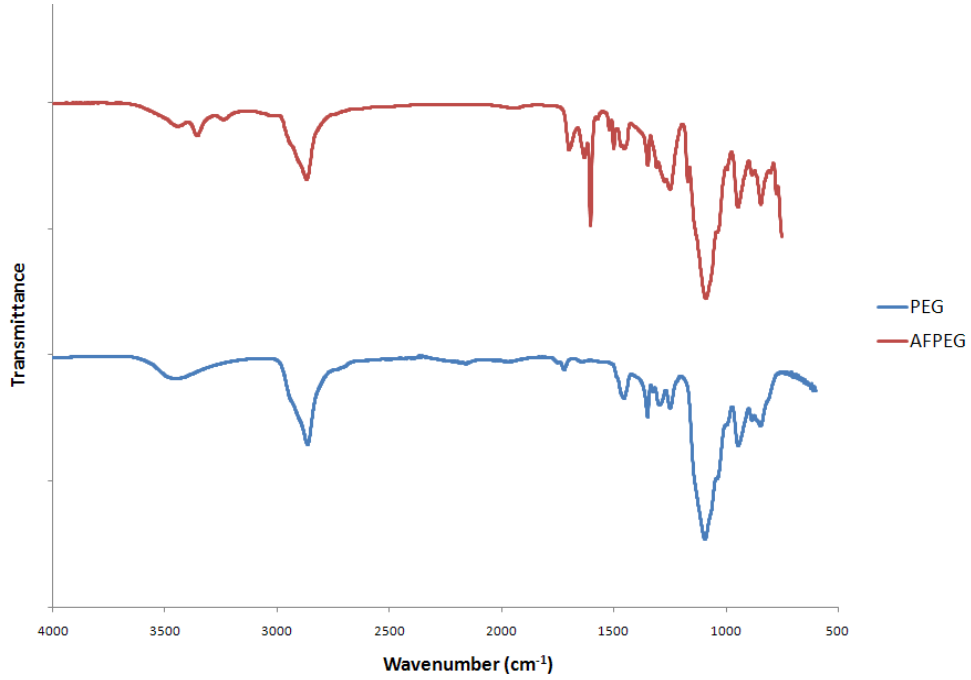

Figure 3.18: A comparison of the FTIR of PEG and amine functionalized PEG

3.2.3. AFPEG/epoxy composites

Dog bone shaped specimens of 5, 10 and 15 phr compositions were prepared for tensile testing by blending aminated polyethylene glycol with epoxy resin followed by adding stochiometric amounts of hardener and curing in silicone moulds for 24 hours. Two sets of specimens were prepared one for AFPEG 600 and the other for AFPEG 1500.

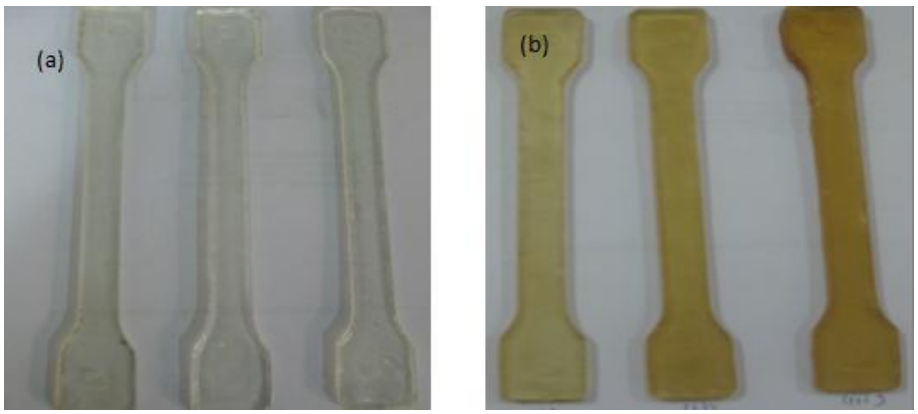

Figure 3.19: Photographs of samples a) neat epoxy b) epoxy composite with AFPEG

3.2.3.1. Thermal characterization

The TG trace of amine functionalized poly ethylene glycol samples are presented in figure 3.19 below. The curves show a one step decomposition pattern in nitrogen atmosphere. The temperature at which decomposition starts i.e. $T_{onset,}$ the final decomposition temperature (T end), the 5% decomposition temperature and T_{max} are shown in table below.

Table 3.5: Results of the thermogravimetric analysis of samples

Sample designation	$T_{5\%}$ (° C)	T_{onset} (° C)	T_{max} (° C)	T_{end} (° C)
EPS	245.4	345.9	365.9	600
AFG65	225.8	344.8	358.7	623.3
AFG610	246.11	345.36	364.22	607.4
AFG615	212.0	341.5	364.1	609.8
AFG155	229.4	343.9	363.3	603.4
AFG1510	220.8	341.3	365.4	602.5
AFG1515	204.1	341.7	362.5	606.4

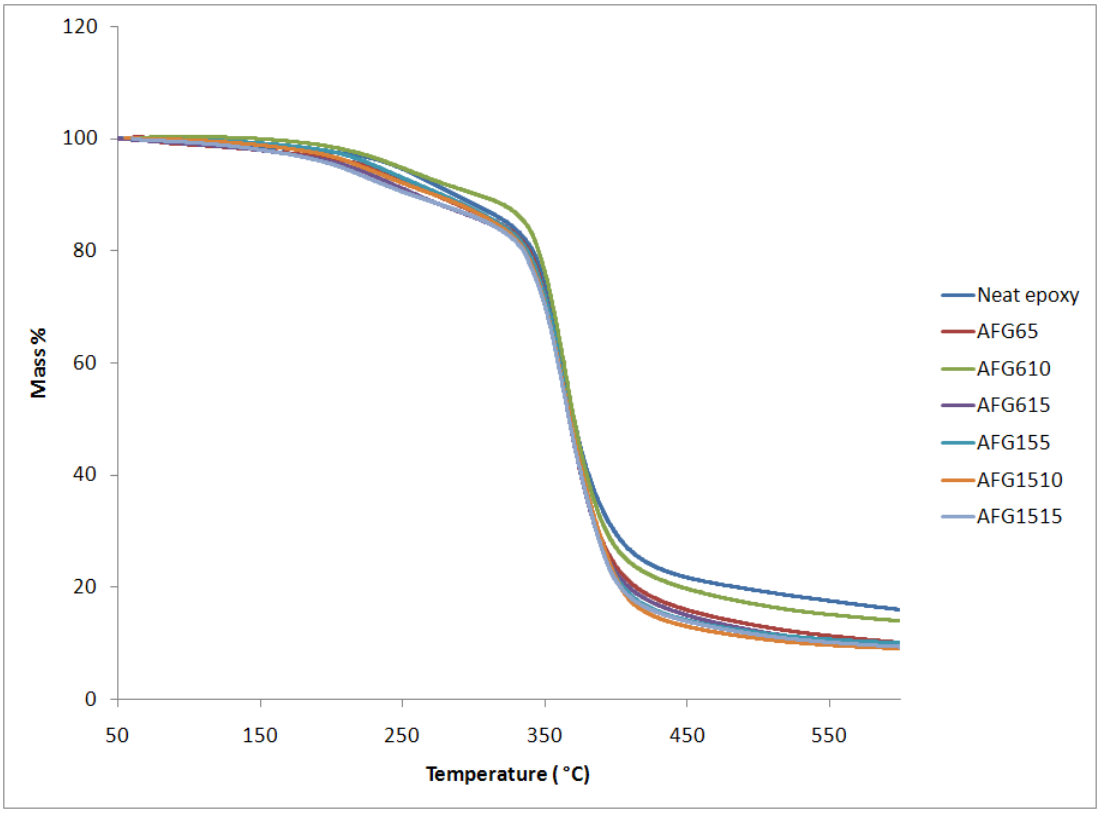

Figure 3.20: TGA curves of neat epoxy and amine terminated PEG samples

3.2.3.2. Quasi-static testing: Tensile testing (ASTM D638)

The tensile testing of the specimen revealed that tensile strength of the samples was sacrificed to a certain extent, when compared to the neat epoxy. However, there was an improvement in the tensile strain which supported our idea of toughening. The figures presented below (Figures 3.21-3.23) show the variation of mechanical properties, due to addition of aminated PEGs.

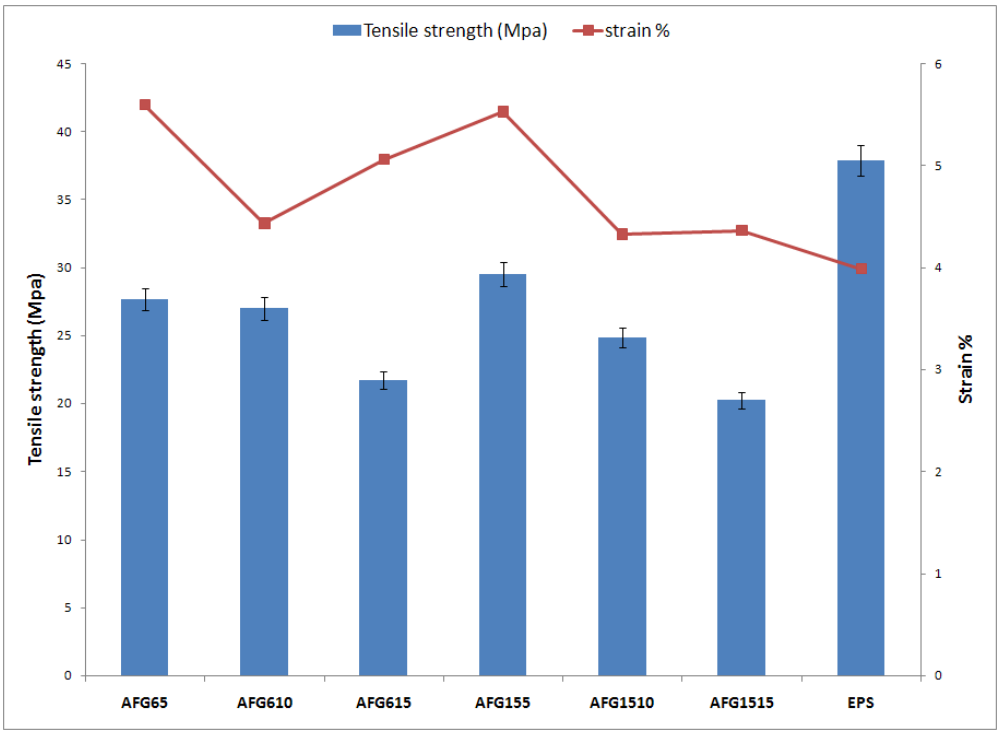

Figure 3.21: Variation in tensile strength and strain % of polymer due to blending with AFPEG

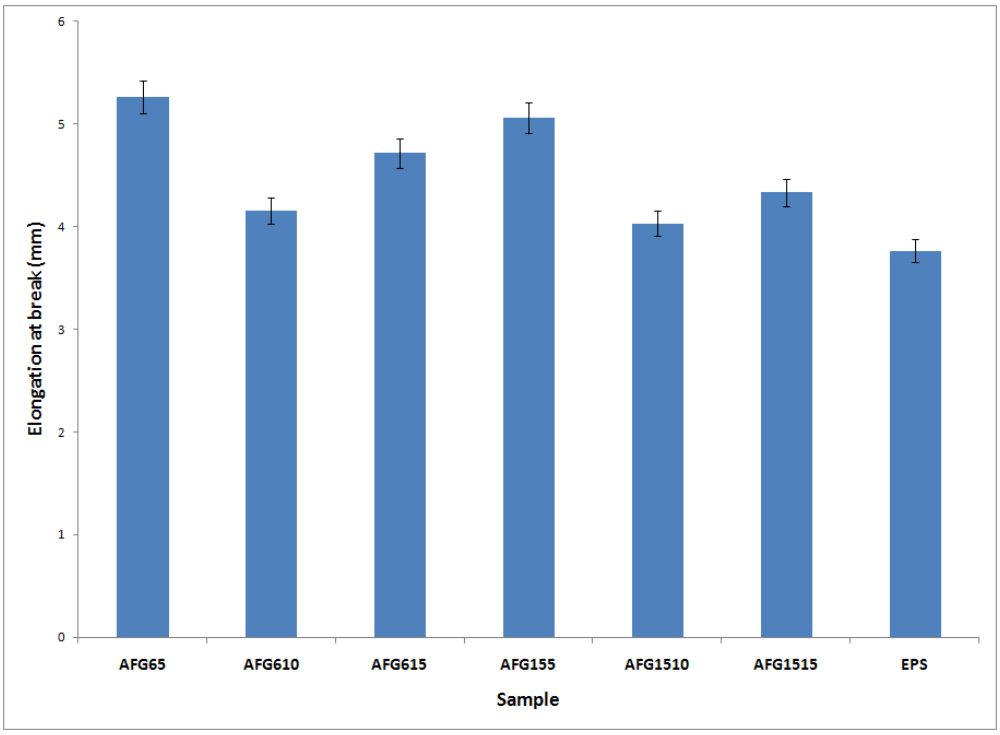

Figure 3.22: Elongation at break of AFPEG samples

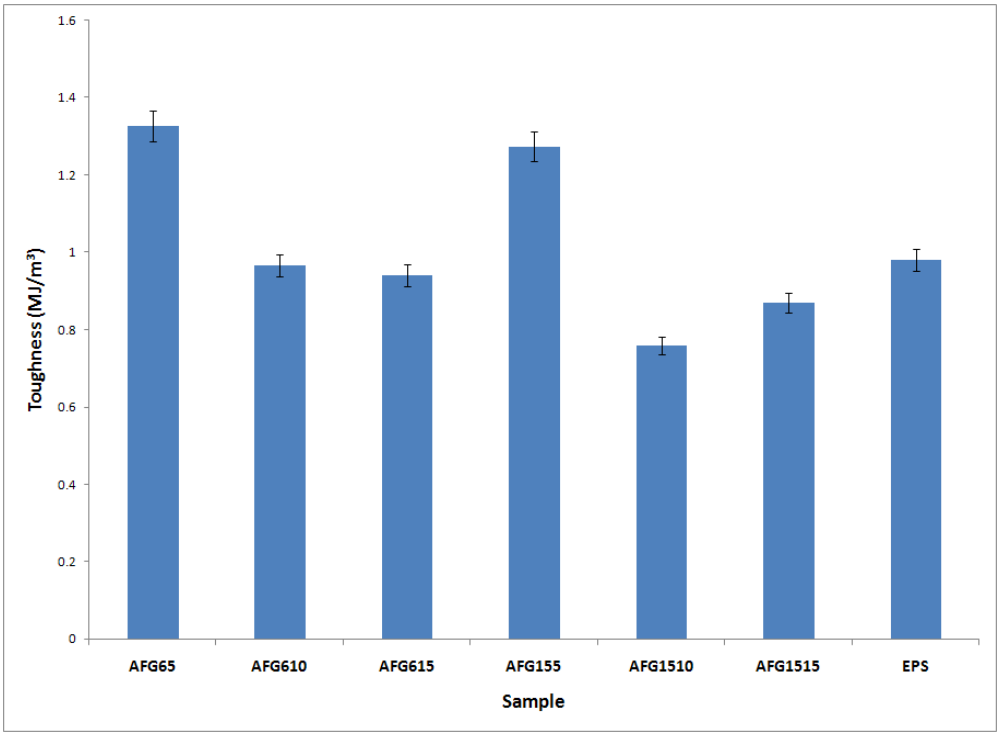

Figure 3.23: Toughness of AFPEG samples

CHAPTER 4

SUMMARY AND CONCLUSIONS

The project deals with improving the toughness of epoxy resins for potential as a retrofitting material on structures in order to reduce the damage that result from the explosion. Attempts have been made in this project to toughen epoxy by use of organic as well as inorganic modifiers.

Toughening by Inorganic mesoporous filler

- Inorganic mesoporous filler (SBA 15) was prepared by polymer templated route and the same was characterized by XRD, FTIR, chemisorption and physisorption analysis, which shows that it has hollow rod like textural properties, with a uniform pore diameter of 5.4 nm combined with a very large BET surface area of 808 m^2/g.

- Epoxy composites were prepared by mixing appropriate amounts of epoxy, hardener and SBA 15 which was added as a reinforcing agent in varying amounts (1-7 % w/w) to strengthen the epoxy matrix.

- These composites were then cured and the mechanical properties i.e. tensile strength, elongation at break, material toughness were determined at low strain rates

- The results revealed that there was a 10-11 percent improvement in toughening on addition of 1% (w/w) SBA 15 in epoxy matrix. However with increase in the amount of loading, the mechanical properties deteriorated a feature which was attributed to the agglomeration of fillers.

- The scanning electron microscopy images of the fractured surfaces of neat epoxy and reinforced epoxy was recorded, which revealed the presence of microcracks. The

studies reveal that the mechanism of failure had changed due to the addition of SBA-15. Neat epoxy fractured in a brittle manner, while the reinforced epoxy exhibited ductile failure.

- High strain rate testing (1000 per second using Split Hopkinson pressure bar) of the samples in compressive mode was performed and the results indicated that the compressive strength of the samples was of the order of 120MPa.

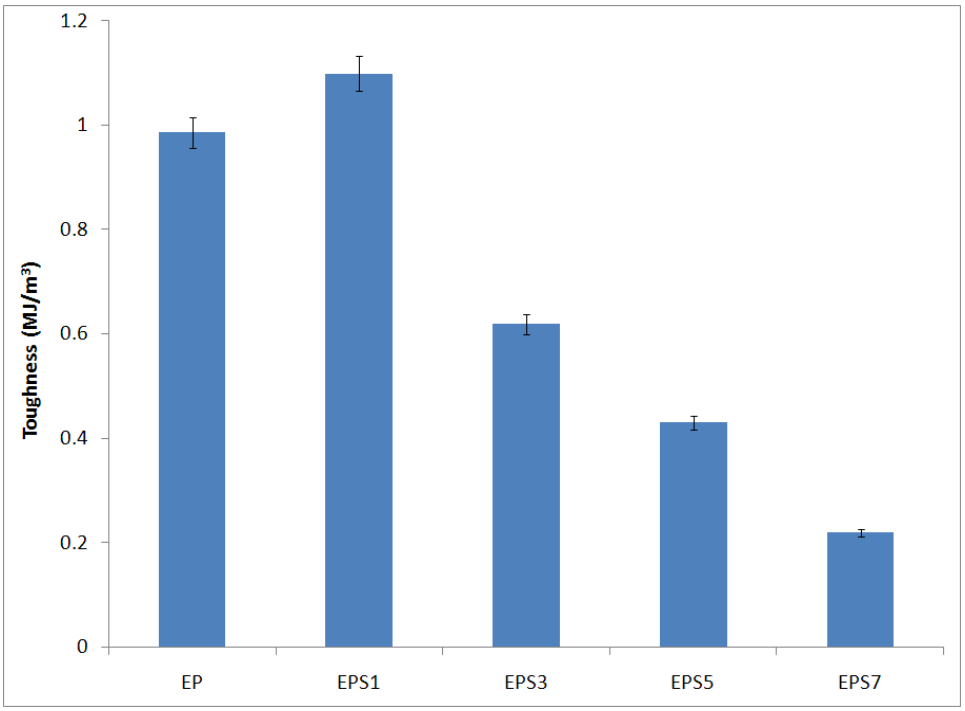

Figure 3.24: An overview of toughness of neat epoxy and SBA 15 reinforced epoxy

Toughening by Organic modifiers

Another route which was adopted towards improving the toughness of the epoxy was by adding organic modifiers. Aminated poly (ethylene glycol) derivatives were used for this purpose.

- PEG of two different molecular weights (M.wt 600 and 1500) were converted to amine terminated PEG 600 (AFG6) amine terminated PEG 1500 (AFG15), by reacting with p-amino benzoic acid.

- The FTIR analysis of the samples revealed the presence of CO-NH bonds in the polymer, which confirmed the conversion of the glycol to its amine derivative.

- The aminated poly (ethylene glycol) was blended with epoxy in 5, 10 and 15 phr concentrations. These were then mixed with hardener and moulded into tensile testing specimens.

- The mechanical properties of the polymer in the tensile mode (quasi static testing) were determined. The results indicated a 37 percent improvement in overall toughness of the polymer as compared to the base sample. However, the tensile strength of the polymer was sacrificed.

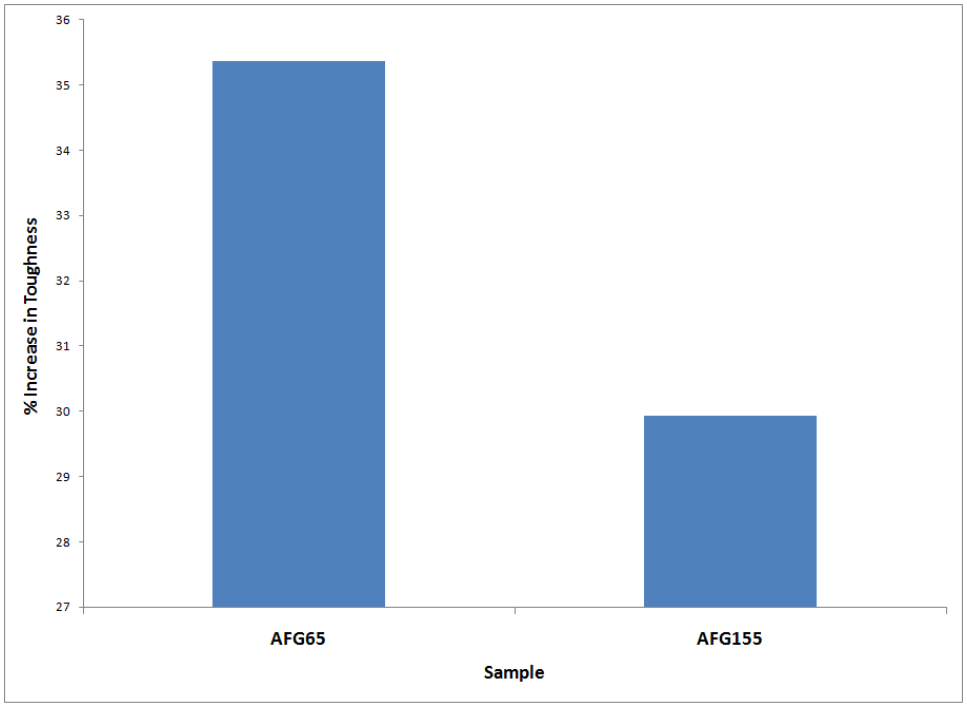

Figure 3.25: Percentage increase in toughness of amine functionalized samples

RECOMMENDATIONS FOR FUTURE WORK

The results obtained so far indicate that epoxy resins can be toughened by addition of mesoporous inorganic fillers and organic modifiers. However, due to time constraints, the behaviour of the material under blast loadings could not be determined. The following studies need to be performed in the future.

- A detailed investigation of the dynamic behaviour of epoxy composites is required to be carried out over a range of temperature and frequencies including creep, stress relaxation and time –temperature superposition as these composites exhibit potential for structural applications.

- It is suggested to conduct quasi static compression test and loading, unloading and reloading of quasi- static tensile specimens to characterize the material behaviour like viscoelasticity and hysteresis.

- Shock tube testing of the composites to investigate the behaviour of the material under blast loads.
- Comparing the Finite Element Analysis modeling results with those obtained by blast loadings.
- Impact strength testing and shock tube testing of organically modified epoxy samples.

APPENDIX 2.1

2.1.1. Determination of epoxy equivalent

For the purpose of quantification of epoxy equivalent, a known amount of epoxy resin (~ 0.5 g) was refluxed with 25 ml of pyridine hydrochloride solution (6.25 ml of conc. HCl (12 M) in 250 mL freshly distilled pyridine) for a period of 20 min, which led to the formation of a transparent solution. Post-cooling, the contents were titrated against previously standardized potassium hydroxide solution (0.2 M) using phenolphthalein as an indicator. The end point was determined by the appearance of pink colour. The reading was noted as T2. A blank experiment was performed first in the absence of epoxy resin (recorded as T1) and the difference between the two sets (i.e., T1-T2) was used to quantify the epoxy content as per the following formula

The epoxy equivalent was calculated from (T1-T2) keeping in view that-

1 ml of 0.2 moles per litre potassium hydroxide = 0.0086 grams epoxide group

Therefore, epoxy equivalent = grams of polymer requiring 5000 ml of 0.2 moles per litre.

The epoxy equivalent was calculated to be 200 g/eq

2.1.2. Determination of total amine content

The total amine content (eq/kg) of the hardener was determined by titration method. A pre-weighed amount of hardener (0.3g) was dissolved in 1:1 water-isopropanol mixture (30 mL) and was subsequently titrated against 1.1 N hydrochloric acid. Bromophenol blue was added as the indicator. The end point of titration was determined by appearance of a yellow colour which increased on further addition of HCl.

. The total moles of amine per gram were determined using the following formula:

$$\text{Amine content} = \frac{\text{volume of HCl (ml)} \times \text{Normality}}{\text{Amount of sample (g)} \times 1000}$$

The total amine content was found out to be 32 eq/kg.

The amine content is usually quantified by any of the following:

Amine Hydrogen Equivalent Weight (AHEW g/eq): This is more commonly referred to as equivalent weight per active Hydrogen, and is defined as the amount (g) of hardener containing one equivalent of N-H groups. This is calculated as Mw of the hardener divided by the number of active hydrogen per molecule

Parts per Hundred Resin (phr): It is defined as the grams of hardener needed per hundred grams of epoxy resin

Conversion: phr = (AHEW * 100) / EEW

Amine Value (Aminzahl): It is also sometimes called amine-index and is defined as milligrams of KOH equivalent to one gram of hardener.

Conversion: NO CORRELATION WITH AHEW

Amine content (Aminwert): It is given by equivalents of N-H per kg of hardener

Conversion: Amine content = 1000 / AHEW

2.1.1. Amount of hardener (HY 951) used

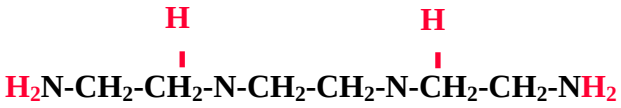

Figure 3.26: TETA, a typical hardener

Molecular weight of the hardener = 146

No of active hydrogen per molecule = 6

Therefore, amine hydrogen equivalent weight (AHEW) = 146/6= 24 g/eq

Epoxy equivalent weight (EEW) = 200 g/eq

$$phr = \frac{AHEW}{EEW} \times 100$$

phr = (24*100)/200 = 12

APPENDIX 3.1.

Weight of sample = 2.5g

Temperature of adsorption = 77K

Slope of BET Plot = $1.5 \times 10^{-3}/cm^3$

Intercept of BET Plot = $0.3 \times 10^{-3}/cm^3$

Ans. BET Surface Area $= \dfrac{(CSA \times 6.023 \times 10^{23})}{22414\ cm^3\ STP \times 10^{18}\ Nm^2/m^2 \times (S + Y_{int})}$

$$= \frac{(0.162\ Nm^2 \times 6.023 \times 10^{23})}{22414\ cm^3\ STP \times 10^{18}\ Nm^2/m^2 \times (1.5 \times 10^{-3}\ g/cm^3 + 0.3 \times 10^{-3}\ g/cm^3)} = \frac{0.975726 \times 10^{23}}{40345.2 \times 10^{15}}$$

$$= \frac{0.975726 \times 10^{23}}{40345.2 \times 10^{15}} = 2.418 \times 10^3\ m^2/g$$

In plotting x/V (1-x) versus x (where $x = p/p^o$) the range of x from 0.05 to 0.30 is selected because mainly it is assumed that in that range the monolayer adsorption is complete. Secondly, this is the relative pressure region in which BET model is found to be valid for all mesoporous sample and this is the multilayer region considered to be valid for BET.

REFERENCES

1. Irshidat, M., et al. *Blast Resistance of Unreinforced Masonry (URM) Walls Retrofitted with Nano Reinforced Elastomeric Materials*. 2009. Austin, Texas: ASCE.
2. Irshidat, M., et al. *Blast Vulnerability Evaluation of Concrete Masonry Unit Infill Walls Retrofitted with Nano Particle Reinforced Polyurea: Modelling and Parametric Evaluation*. 2011. Las Vegas, NV: ASCE.
3. Cullis, I.G., J. Schofield, and A. Whitby, *Assessment of blast loading effects – Types of explosion and loading effects.* International Journal of Pressure Vessels and Piping, 2010. **87**(9): p. 493-503.
4. Kinney, G.F. and K.J. Graham, *Explosive Shocks in Air*. 2 ed. 1985, Berlin: Springer-Verlag Berlin and Heidelberg GmbH & Co. KG.
5. *Federal Emergency Management Agency, Reference Manual to Mitigate Potential Terrorist Attacks Against Buildings, Risk Management Series no 426*. December 2003: Washington, D.C.
6. John J. Myers1, A.B., and Khaled A. El-Domiaty3, *Blast Resistance of Frp Retrofitted Un-Reinforced Masonry (URM) Walls With and Without Arching Action.* tms, august 2004.
7. Myers, J.J., A. Belarbi, and K.A. El - Domiaty, *Blast resistance of FRP Retrofitted Un-Reinforced Masonary (URM) Walls With and Without Arching Action.* The Masonry Society, 2004: p. 9-26.
8. Roland, C.M., D. Fragiadakis, and R.M. Gamache, *Elastomer–steel laminate armor.* Composite Structures, 2010. **92**(5): p. 1059-1064.
9. *Blast resistance of polyurea based layered composite materials.* Composite Structures, 2008. **84**(3): p. 271.
10. Tekalur, S.A., A. Shukla, and K. Shivakumar, *Blast resistance of polyurea based layered composite materials.* Composite Structures, 2008. **84**(3): p. 271-281.
11. Grujicic, M., et al., *Fluid/Structure Interaction Computational Investigation of Blast-Wave Mitigation Efficacy of the Advanced Combat Helmet.* Journal of Materials Engineering and Performance, 2011. **20**(6): p. 877-893.
12. Grujicic, M., et al., *Blast-wave impact-mitigation capability of polyurea when used as helmet suspension-pad material.* Materials & Design, 2010. **31**(9): p. 4050-4065.
13. Grujicic, M., et al., *Shock-Wave Attenuation and Energy-Dissipation Potential of Granular Materials.* Journal of Materials Engineering and Performance, 2012. **21**(2): p. 167-179.
14. Grujicic, M., et al., *Molecular-level simulations of shock generation and propagation in polyurea.* Materials Science and Engineering: A, 2011. **528**(10–11): p. 3799-3808.
15. Grujicic, M., et al., *Spall-Fracture Physics and Spallation-Resistance-Based Material Selection.* Journal of Materials Engineering and Performance: p. 1-11.
16. Grujicic, M., et al., *Computational investigation of impact energy absorption capability of polyurea coatings via deformation-induced glass transition.* Materials Science and Engineering: A, 2010. **527**(29–30): p. 7741-7751.
17. Grujicic, M., et al., *Multi-length scale modeling and analysis of microstructure evolution and mechanical properties in polyurea.* Journal of Materials Science, 2011. **46**(6): p. 1767-1779.
18. Yi, J., et al., *Large deformation rate-dependent stress–strain behavior of polyurea and polyurethanes.* Polymer, 2006. **47**(1): p. 319-329.

19. Amirkhizi, A.V., et al., *An experimentally-based viscoelastic constitutive model for polyurea, including pressure and temperature effects.* Philosophical Magazine, 2006. **86**(36): p. 5847-5866.
20. Sarva, S.S. and A.J. Hsieh, *The effect of microstructure on the rate-dependent stress–strain behavior of poly(urethane urea) elastomers.* Polymer, 2009. **50**(13): p. 3007-3015.
21. May, C.A., ed. *Epoxy Resins Chemistry and Technology*. 2nd ed. 1988, Marcel Dekker: New York.
22. Sandler, S.R., et al., *Epoxy resins*, in *Polymer Synthesis and Characterization*. 1998, Academic Press: San Diego. p. 61-67.
23. Hodd, K., *37 - Epoxy Resins*, in *Comprehensive Polymer Science and Supplements*, A. Editor-in-Chief: Sir Geoffrey, Editor. 1989, Pergamon: Amsterdam. p. 667-699.
24. Hodgkin, J., *Thermosets: Epoxies and Polyesters*, in *Encyclopedia of Materials: Science and Technology (Second Edition)*, K.H.J.B. Editors-in-Chief: , et al., Editors. 2001, Elsevier: Oxford. p. 9215-9221.
25. Takeichi, T. and N. Furukawa, *5.25 - Epoxy Resins and Phenol-Formaldehyde Resins*, in *Polymer Science: A Comprehensive Reference*, M. Editors-in-Chief: Krzysztof and M. Martin, Editors. 2012, Elsevier: Amsterdam. p. 723-751.
26. Kunz-Douglass, S., P.W.R. Beaumont, and M.F. Ashby, *A model for the toughness of epoxy-rubber particulate composites.* Journal of Materials Science, 1980. **15**(5): p. 1109-1123.
27. Kunz, S.C. and P.W.R. Beaumont, *Low-temperature behaviour of epoxy-rubber particulate composites.* Journal of Materials Science, 1981. **16**(11): p. 3141-3152.
28. Kinloch, A., et al., *The effect of silica nano particles and rubber particles on the toughness of multiphase thermosetting epoxy polymers.* Journal of Materials Science, 2005. **40**(18): p. 5083-5086.
29. Hsieh, T., et al., *The toughness of epoxy polymers and fibre composites modified with rubber microparticles and silica nanoparticles.* Journal of Materials Science, 2010. **45**(5): p. 1193-1210.
30. Bucknall, C.B. and I.K. Partridge, *Phase separation in epoxy resins containing polyethersulphone.* Polymer, 1983. **24**(5): p. 639-644.
31. Chen, T.K. and H.J. Shy, *Effects of matrix ductility on rubber/matrix interfacially modified epoxy resins.* Polymer, 1992. **33**(8): p. 1656-1663.
32. Hedrick, J.L., et al., *Chemical modification of matrix resin networks with engineering thermoplastics: 1. Synthesis, morphology, physical behaviour and toughening mechanisms of poly(arylene ether sulphone) modified epoxy networks.* Polymer, 1991. **32**(11): p. 2020-2032.
33. He, X., et al., *Shape and size effects of ceria nanoparticles on the impact strength of ceria/epoxy resin composites.* Particuology, 2011. **9**(1): p. 80-85.
34. Lange, F.F., *The interaction of a crack front with a second-phase dispersion.* Philosophical Magazine, 1970. **22**(179): p. 0983-0992.
35. Evans, A.G., *The strength of brittle materials containing second phase dispersions.* Philosophical Magazine, 1972. **26**(6): p. 1327-1344.
36. Casalini, R., et al., *Nanofiller reinforcement of elastomeric polyurea.* Polymer, 2012. **53**(6): p. 1282-1287.
37. Ye, Y., et al., *High impact strength epoxy nanocomposites with natural nanotubes.* Polymer, 2007. **48**(21): p. 6426-6433.
38. Sun, L., et al., *Energy absorption capability of nanocomposites: A review.* Composites Science and Technology, 2009. **69**(14): p. 2392-2409.

39. Reda Taha, M.M., A.B. Colak-Altunc, and M. Al-Haik, *A multi-objective optimization approach for design of blast-resistant composite laminates using carbon nanotubes.* Composites Part B: Engineering, 2009. **40**(6): p. 522-529.
40. Iqbal, K., et al., *Impact damage resistance of CFRP with nanoclay-filled epoxy matrix.* Composites Science and Technology, 2009. **69**(11–12): p. 1949-1957.
41. Bekyarova, E., et al., *Multiscale Carbon Nanotube−Carbon Fiber Reinforcement for Advanced Epoxy Composites.* Langmuir, 2007. **23**(7): p. 3970-3974.
42. Liu, X., et al., *Blast resistance of sandwich-walled hollow cylinders with graded metallic foam cores.* Composite Structures, (0).
43. Hoffmann, F., et al., *Silica-Based Mesoporous Organic—Inorganic Hybrid Materials.* ChemInform, 2006. **37**(34): p. no-no.
44. Suzuki, N., S. Kiba, and Y. Yamauchi, *Bimodal filler system consisting of mesoporous silica particles and silica nanoparticles toward efficient suppression of thermal expansion in silica/epoxy composites.* Journal of Materials Chemistry, 2011. **21**(38): p. 14941-14947.
45. Suzuki, N., S. Kiba, and Y. Yamauchi, *Fabrication of mesoporous silica/polymer composites through solvent evaporation process and investigation of their excellent low thermal expansion property.* Physical Chemistry Chemical Physics, 2011. **13**(11): p. 4957-4962.
46. Ji, X., et al., *Mesoporous Silica-Reinforced Polymer Nanocomposites.* Chemistry of Materials, 2003. **15**(19): p. 3656-3662.
47. Jiao, J., X. Sun, and T.J. Pinnavaia, *Mesostructured silica for the reinforcement and toughening of rubbery and glassy epoxy polymers.* Polymer, 2009. **50**(4): p. 983-989.
48. Lin, J. and X. Wang, *Preparation, microstructure, and properties of novel low-κ brominated epoxy/mesoporous silica composites.* European Polymer Journal, 2008. **44**(5): p. 1414-1427.
49. Lin, J. and X. Wang, *Novel low-κ polyimide/mesoporous silica composite films: Preparation, microstructure, and properties.* Polymer, 2007. **48**(1): p. 318-329.
50. He, J., et al., *Nanocomposite Structure Based on Silylated MCM-48 and Poly(vinyl acetate).* Chemistry of Materials, 2003. **15**(20): p. 3894-3902.
51. Zhang, F.-A., D.-K. Lee, and T.J. Pinnavaia, *PMMA/mesoporous silica nanocomposites: effect of framework structure and pore size on thermomechanical properties.* Polymer Chemistry, 2010. **1**(1): p. 107-113.
52. Kojima, Y., T. Matsuoka, and H. Takahashi, *Preparation of nylon 66/mesoporous molecular sieve composite under high pressure.* Journal of Applied Polymer Science, 1999. **74**(13): p. 3254-3258.
53. Chen, Z., et al., *Effects of mesoporous SBA-15 contents on the properties of polystyrene composites via in-situ emulsion polymerization.* Journal of Polymer Research, 2012. **19**(3): p. 1-8.
54. Nakajima, H., et al., *Preparation and characterization of polypropylene/mesoporous silica nanocomposites with confined polypropylene.* Journal of Polymer Science Part B: Polymer Physics, 2003. **41**(24): p. 3324-3332.
55. Meynen, V., P. Cool, and E.F. Vansant, *Verified syntheses of mesoporous materials.* Microporous and Mesoporous Materials, 2009. **125**(3): p. 170-223.
56. Samanta, B.C., et al., *Toughening of Epoxy Resin with Solid Amine Terminated Poly (ethylene glycol) Benzoate and Effect of Red Mud Waste Particles.* Journal of material science and technology, 2008. **24** (02): p. 272-278.
57. Sing, K.S.W., *Reporting physisorption data for gas/solid systems with special reference to the determination of surface area and porosity* Pure and Applied chemistry, 1982. **54**(11): p. 2201-2218.

58. Naskar, M.K. and M. Eswaramoorthy, *Significant improvement in the pore properties of SBA-15 brought about by carboxylic acids and hydrothermal treatment.* Journal of Chemical Sciences, 2008. **120**(1): p. 181–186.
59. Sauer, J. and J.-R. Hill, *The acidity of surface silanol groups. A theoretical estimate based on ab initio calculations on a model surface.* Chemical Physics Letters, 1994. **218**(4): p. 333-337.
60. Chen, J.-S., et al., *Controlled degradation of epoxy networks: analysis of crosslink density and glass transition temperature changes in thermally reworkable thermosets.* Polymer, 2004. **45**(6): p. 1939-1950.
61. Alamri, H. and I.M. Low, *Effect of water absorption on the mechanical properties of nano-filler reinforced epoxy nanocomposites.* Materials and Design.
62. Vogt, J., *Thermal analysis of epoxy-resins: Identification of decomposition products.* Thermochimica Acta, 1985. **85**(0): p. 411-414.
63. Romanes, M.C., et al., *Surface and subsurface characterization of epoxy-mesoporous silica composites to clarify tribological properties.* Wear, 2008. **265**(1–2): p. 88-96.
64. Suzuki, N., S. Kiba, and Y. Yamauchi, *Fabrication of Epoxy Composites with Large-Pore Sized Mesoporous Silica and Investigation of Their Thermal Expansion.* Journal of Nanoscience and Nanotechnology, 2012. **12**(2): p. 983-987.